ENTER

FLOW IN POLYCRYSTALLINE ICE

By

Chris Wilson and Brett Marmo

School of Earth Sciences, The University of Melbourne

Victoria 3010, Australia

Created and maintained by Hadi Sim.

School of Earth Sciences

The University of Melbourne

Victoria 3010, Australia

Last updated: 6th March 2000

Home

FLOW IN POLYCRYSTALLINE ICE

By Chris Wilson and Brett Marmo

Abstract - Polycrystalline ice can accommodate large amounts of intracrystalline plastic deformation and in so doing develops specific flow characteristics and crystallographic preferred orientations. Ice flow at the scale of an ice crystal is dominated by the anisotropic nature of the crystal, with its dominant slip system in the basal plane. Polar ice tends to develop a preferred bulk fabric in response to its stress, strain rate and temperature history as it ages in cold ice sheets. Deformation is localised at the base of ice sheets, so the crystallographic fabric becomes progressively more pervasive with depth, with preferred vertical c-axis fabrics. This means that the anisotropic behaviour during flow is also manifested at scales larger than the ice grains as ice becomes progressively harder to compress vertically, and easier to shear horizontally with the development of contrasting brittle-ductile regimes.

Time-lapse images photographed through an optical microscope are presented which demonstrate intracrystalline processes associated with the deformation of granular ice aggregates in either a pure shear or simple shear. Sequences show that contemporaneous with these processes are dynamic recrystallisation, which involves nucleation of equiaxed grains, the motion of grain boundaries and the development of a preferred dimensional orientation. Underlying this deformation is the movement of dislocations and the generation of defect structures that contribute to the creep behaviour in polycrystalline ice. However, single crystals of ice have a very strong plastic anisotropy, as glide is several orders of magnitude easier on basal systems than on non-basal systems. An analogy is made to other hexagonal minerals such as quartz where the most commonly reported slip system is in the basal plane.

When polycrystalline ice is subjected to stress the deformation of individual grains is blocked by neighbouring grains and this builds up internal stresses both in the deforming grains and those around them. These stresses can be relieved in a variety of ways, all of which play some part in the deformation, namely:

1. Non-uniform deformation within a single grain can produce bending and the formation of undulose extinction or kinking.

2. Grains may slide over one another and microcracks may be nucleated.

3. Grain boundary migration will occur, causing some grains to grow at the expense of others. This process requires diffusion-controlled recovery, and may accompany the intracrystalline glide.

4. In regions which are highly deformed recrystallisation occurs, with the nucleation and subsequent growth of new grains, often more favourably oriented for basal slip. This can occur repeatedly during deformation, and is known as dynamic recrystallisation; this is accelerated by a decrease in grain size and where the initial orientation of grains are at a maximum critical resolved shear stress.

Table of contents | List of figures | Main text

Wilson, C. and Marmo, B. 2000. Flow in Polycrystalline Ice. In: Stress, Strain and Structure, A volume in honour of W D Means. Eds: M.W. Jessell and J.L.Urai. Volume 2, Journal of the Virtual Explorer. ISSN 1441-8126 (Print). ISSN 1441-8134 (CD-ROM). ISSN 1441-8126 (On-line at www.virtualexplorer.com.au/VEjournal/Volume2).

Home

FLOW IN POLYCRYSTALLINE ICE

By Chris Wilson and Brett Marmo

Contents

Home

FLOW IN POLYCRYSTALLINE ICE

By Chris Wilson and Brett Marmo

List of figures

Antarctica (Marmo & Wilson 1998).

Figure 1.6.2: Longitudinal section parallel to the flow lines in the Framnes Mountains glacier.

Figure 1.6.3: Divergent, parallel and convergent flow regimes and observed *c*-axes fabric associated with each.

Figure 2.1.1: In-situ simple shear deformation apparatus.

Figure 2.1.2: Plan view of in-situ pure shear deformation apparatus.

Figure 2.2.1: Simulated fabric development in flow lines from an outlet glacier in the Framnes Mountains, Antarctica.

Figure 2.3.1: The crystal structure of ice Ih, showing the arrangement of molecules projected onto the $(10\bar{1}0)$ plane.

Figure 2.3.2: The propagation of a dislocation through the basal plane of an ice lattice.

Figure 2.5.1: A Frank-Read source for the multiple initiation of dislocation loops.

Figure 2.6.1: The Ice Ih lattice.

Figure 2.8.1: When a cantilever is applied to a single crystal of ice the deformation style is dependent on the orientation of the basal plane relative to the load.

Figure 2.9.1: Creep curves in ice.

Figure 2.9.2: A schematic sketch of stress-time curve for deformation in a single crystal of ice at -10°C.

Figure 2.10.1: Two separated portions of a crystal showing a model for calculating the resolved shear stress in a single-crystal specimen.

Figure 2.11.1: Data for glide on basal and non-basal systems, and in isotropic polycrystalline ice compiled by Duval et al, (1983).

Figure 2.14.1: Schematic creep curve for polycrystalline ice under constant

load.

Figure 2.15.1: Plots of strain rate as a function of strain for creep of granular polycrystalline ice in uniaxial compression under various stresses.

Figure 2.15.2: The minimum strain rate is uniaxial creep tests on granular polycrystalline ice as functions of stress at various temperatures.

Figure 2.17.1: Deformation mechanism maps for isotropic polycrystalline ice by Goodman et al. (1981).

Figure 2.19.1: Grain size reduction occurs in a shear zone developed in coarse ice deformed at -2°C.

Home

FLOW IN POLYCRYSTALLINE ICE

Part 1 - Examples of microscopic flow

By Chris Wilson and Brett Marmo

1.1 Introduction

Experimental modelling to illustrate the development of microstructures at high metamorphic grade is inherently difficult due to the paucity of information concerning the rheology of polyphase rocks in the Earth's crust. Conversely, the rheology of ice, even close to its melting point, is very well known and provides an excellent material to model a dynamic system.

A proper interpretation of the origins of microstructure and microstructural dynamics is fundamental to our understanding of the flow in rocks and in ice masses such as glaciers. Glacial ice and rock at high metamorphic grade deform according to the same non-linear flow laws. Ice is therefore an ideal analogue for the study of crustal deformation. Folds, faults, boudinage structures and shear zones can be observed in glaciers at both the mesoscale and macroscale. It is also possible to directly measure the strain rate associated with the development of structures in glaciers. The integration of strain rate measurements with constitutive flow laws and an understanding of material parameters allows us to interpret the flow of polycrystalline materials.

- This is a deforming ice mass, that is viewed under a microscope and photographed in plane polarised light using time lapse photography.

- The processes we see occur as solid state transformations and involve submicroscopic interactions between

Movie 1 - Pure shear deformation in polycrystalline ice over ≈ 2.5 days.

Click on the image to see the movie. It takes a few minutes to download. So please be patient.

dislocations, and differently oriented grain boundaries in a variety of misoriented grains with respect to the applied stress axis.

- These are referred to as intracrystalline processes and involve the generation of defect structures in the crystal lattice as a result of the deformation.

The flow of rock and on the scale of a crystal is dominated by the anisotropic nature of the crystal structure; in hexagonal minerals such as quartz (Fig. 1.1.1) and ice (Fig. 1.1.2) the most commonly reported slip system is in the basal plane (0001). Basal glide will only occur if the critical resolved shear stress on the potential glide plane is sufficiently low to activate three-dimensional glide. Diffusional flow is another process that operates at high temperatures.

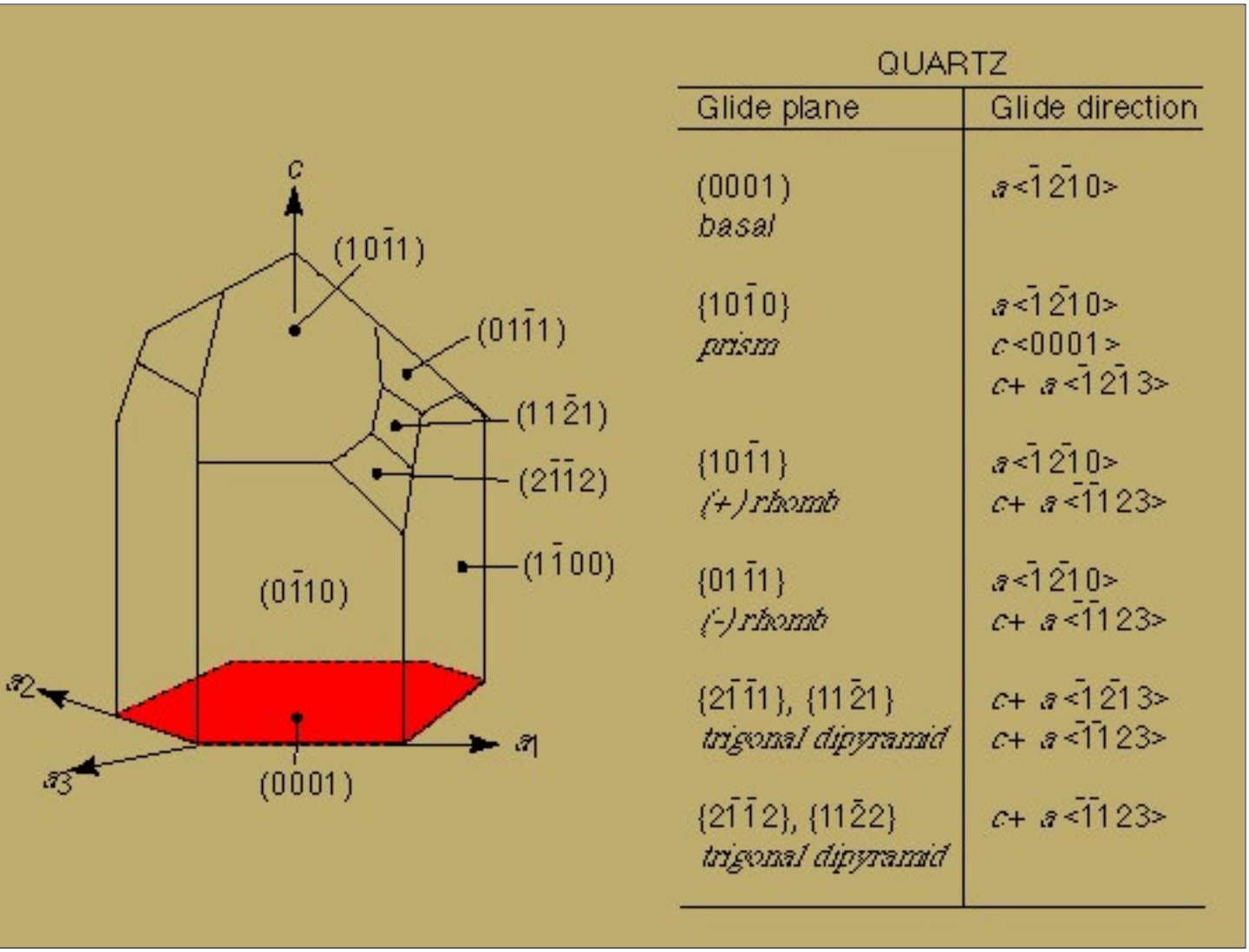

QUARTZ

Glide plane	Glide direction
(0001) *basal*	$a\langle\bar{1}\bar{2}10\rangle$
{10$\bar{1}$0} *prism*	$a\langle\bar{1}\bar{2}10\rangle$ $c\langle0001\rangle$ $c+a\langle\bar{1}\bar{2}\bar{1}3\rangle$
{10$\bar{1}$1} *(+) rhomb*	$a\langle\bar{1}\bar{2}10\rangle$ $c+a\langle\bar{1}\bar{1}23\rangle$
{01$\bar{1}$1} *(-) rhomb*	$a\langle\bar{1}\bar{2}10\rangle$ $c+a\langle\bar{1}\bar{1}23\rangle$
{2$\bar{1}\bar{1}$1}, {11$\bar{2}$1} *trigonal dipyramid*	$c+a\langle\bar{1}\bar{2}\bar{1}3\rangle$ $c+a\langle\bar{1}\bar{1}23\rangle$
{2$\bar{1}\bar{1}$2}, {11$\bar{2}\bar{2}$} *trigonal dipyramid*	$c+a\langle\bar{1}\bar{1}23\rangle$

Figure 1.1.1: Quartz crystal showing location of main crystal faces and principal crystallographic axes. The table lists some of the potential glide systems in quartz.

- It should be noted that not all slip systems will be activated as the critical resolved shear stress of many of these systems will be too high to prevent activation of the system.
- As the critical resolved shear-stress is very low on (0001) then deformation is dominated by slip on the basal plane.
- Additional independent glide can occur on non-basal systems and include various combinations parallel to an *a*-axis, *c*-axis or one of the vector sums *c*+*a* and these are particularly important in the higher temperature deformation of minerals such as quartz (Fig. 1.1.1).

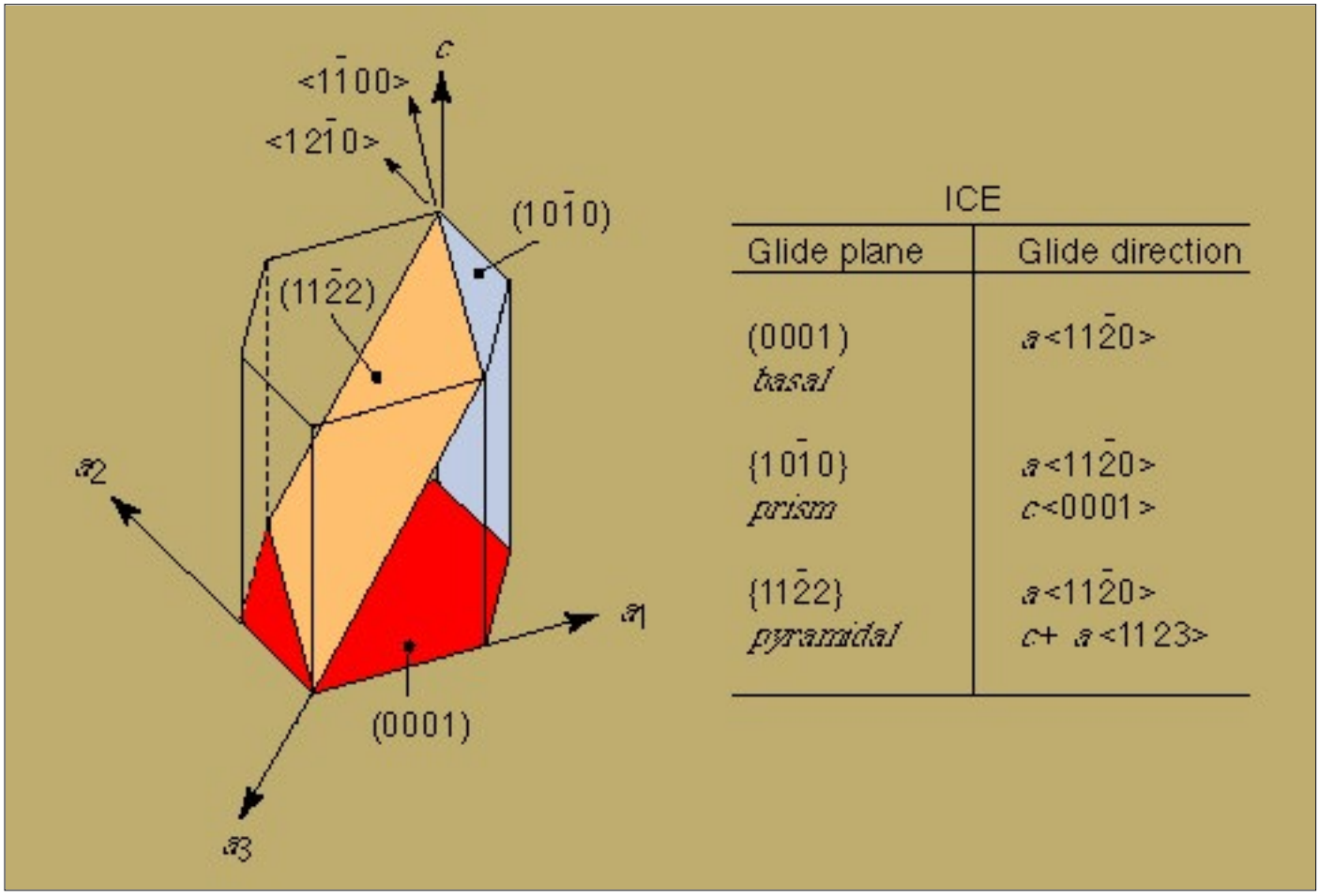

ICE

Glide plane	Glide direction
(0001) *basal*	*a*<11$\bar{2}$0>
{10$\bar{1}$0} *prism*	*a*<11$\bar{2}$0> *c*<0001>
{11$\bar{2}$2} *pyramidal*	*a*<11$\bar{2}$0> *c*+ *a*<11$\bar{2}$3>

Figure 1.1.2: Schematic representation of the basal glide plane (0001) in ice in relation to non-basal glide planes and glide directions.

Because of their low crystallographic symmetry and their limited glide systems it is possible to make comparisons between the microstructural behaviour of quartz (Fig. 1.1.1) and ice (Fig. 1.1.2) when undergoing plastic deformation. For instance if a single crystal is flattened it will shear by intracrystalline glide on its basal plane; this produces a shape transformation and a rotation of its *c*- axis (Fig. 1.1.3). A crystal can be considered as a matrix of elastic-plastic glide planes belonging to the one slip system, which will follow elastic-plastic behaviour and will only be activated if it reaches a critical value of resolved shear-stress.

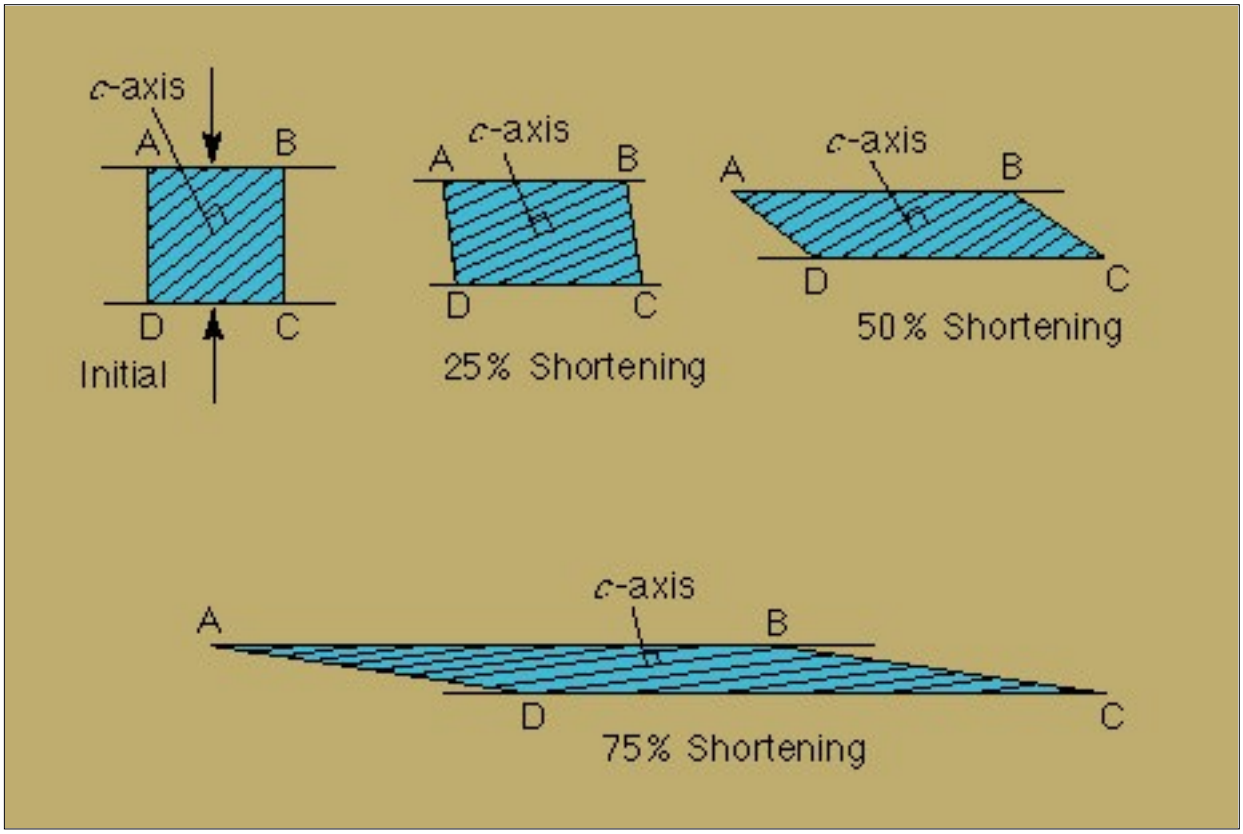

Figure 1.1.3: The flattening of a single crystal that accommodates the shortening by shearing on its basal plane in which the initial critical resolved shear-stress will be high as it lies approximately 45° to the compression direction.

1.2 Polycrystalline aggregates deformed in pure-shear

The simplest deformation that we can consider is a pure shear (Fig. 1.2.1) where there is no rotation of the principal strain axes.

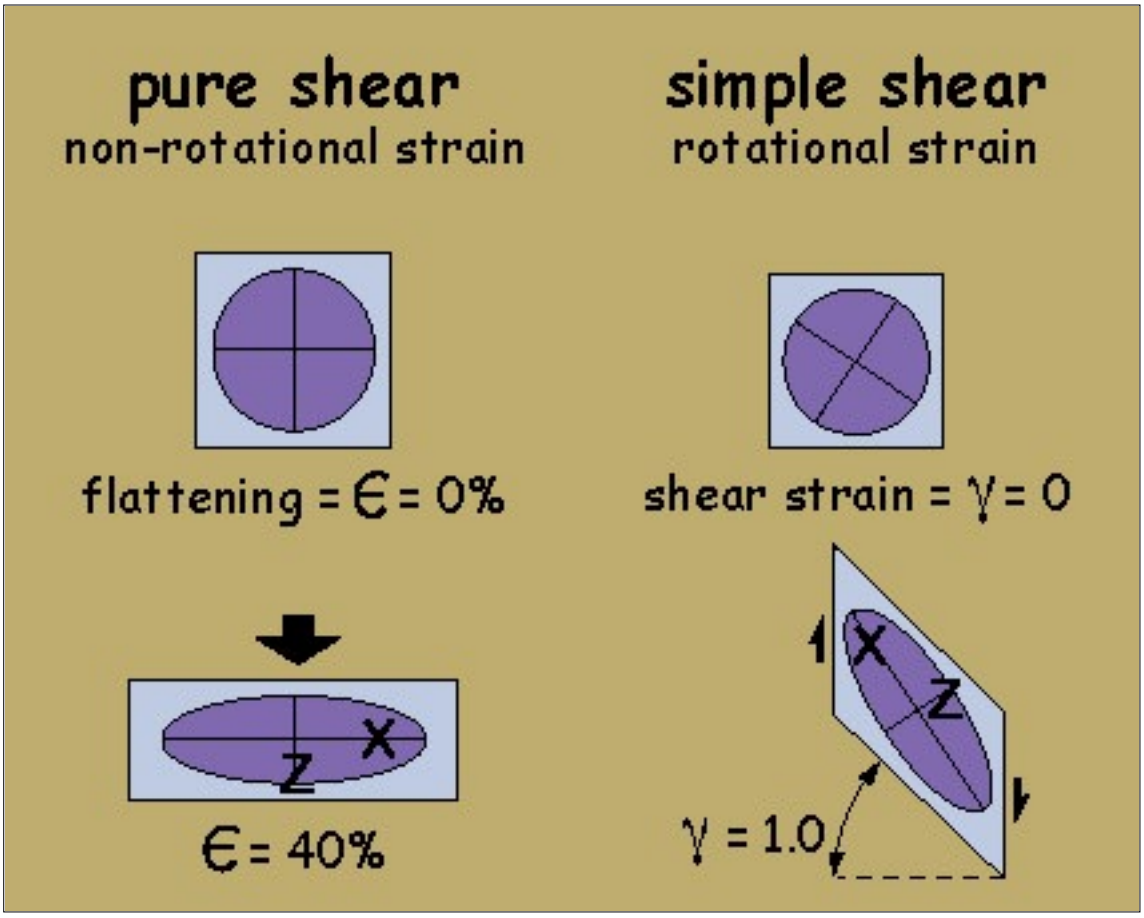

Figure 1.2.1: A Pure shear deformation

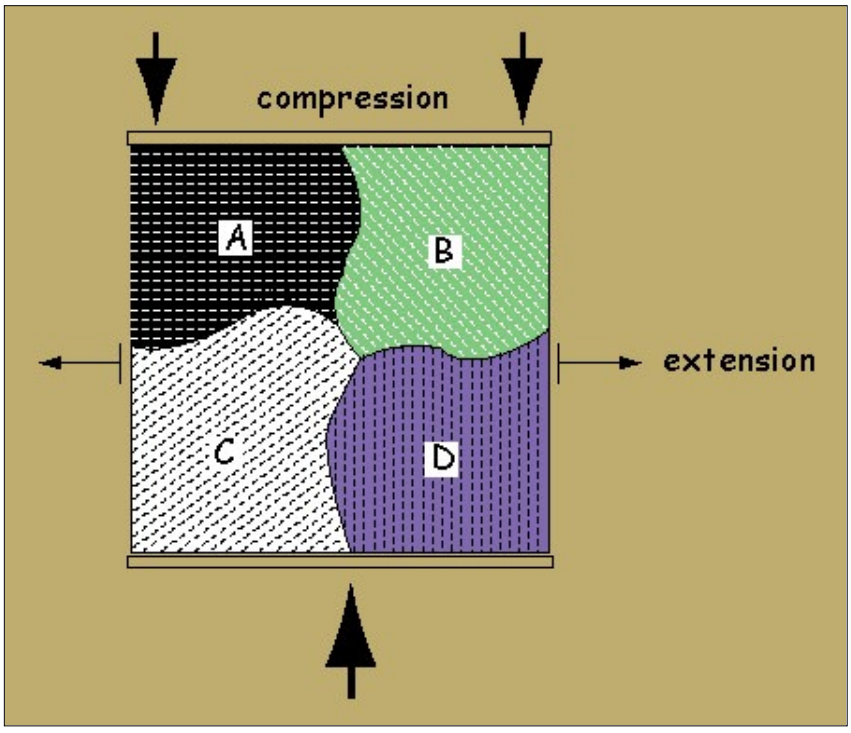

Figure 1.2.2: Two dimensional representation of four undeformed polygonal grains (A, B, C and D) with basal planes (0001) indicated by broken lines being deformed in a pure shear regime. These basal planes are oriented at high-angle to the viewing plane.

- Rocks are composed of densely packed collections of single crystals that comprises a polycrystalline grain aggregate. Each crystal grain contains an infinite number of glide planes which will be activated for slip when the resolved shear stress on the glide plane is equal to the critical resolved shear stress.

To ensure homogeneous deformation of a polycrystalline material, in three-dimensions, 5 independent slip systems are necessary as specified by the Taylor-von Mises criteria (see Taylor, 1938). In ice the basal plane provides only 2 slip systems while the non-basal systems are at least 2-3 orders of magnitude harder to activate. Consequently, the stresses and strain rates for glide on basal systems are different in each grain. The deviation of local behaviour with respect to macroscopic behaviour depends on the directional viscoplastic properties of the grains and the whole polycrystal.

The glide planes that will be first activated upon deformation will occupy orientations that have high critical resolved shear-stresses on the basal planes (Fig. 1.2.2, grains B and C), these are the easy-glide planes, and have orientations at approximately 45° to the bulk compression axis.

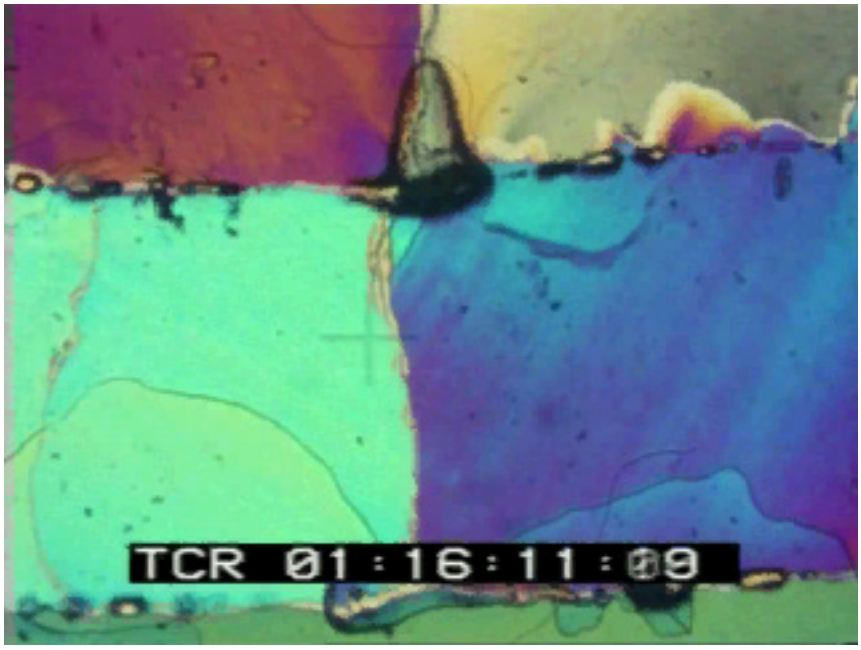

Movie 2 - Pure shear deformation over ≈ 6 days.

Click on the image to see the movie. It takes a few minutes to download. So please be patient.

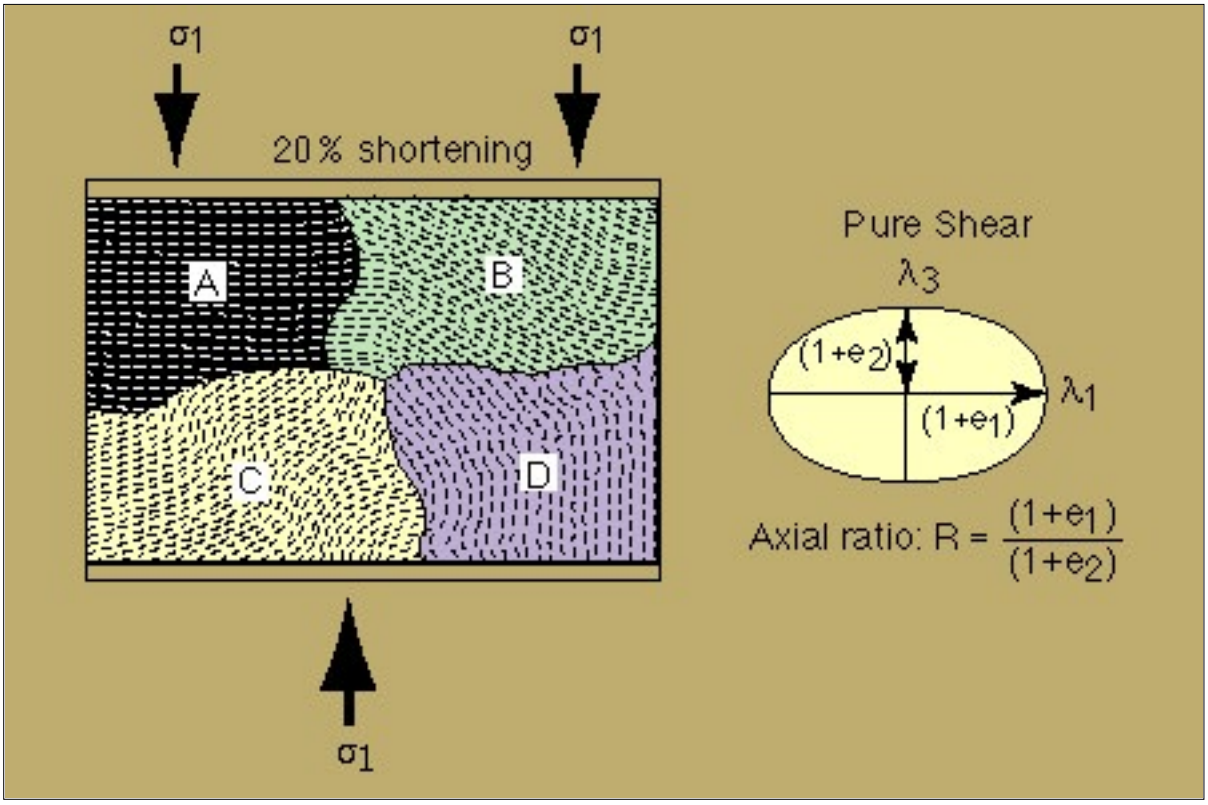

Figure 1.2.3: A pure-shear deformation with 20% bulk shortening and showing the relationship to the finite strain ellipse.

Grains in easy-glide orientations (Fig. 1.2.3, grains B and C) will be activated first and then produce bending of the (0001) as they try to accommodate for the strain in their neighbouring grains. Grain A is in hard-glide orientation and would undergo flattening and extension. Whereas Grain D undergoes only limited glide, but as it lies parallel to the bulk compression direction it will kink.

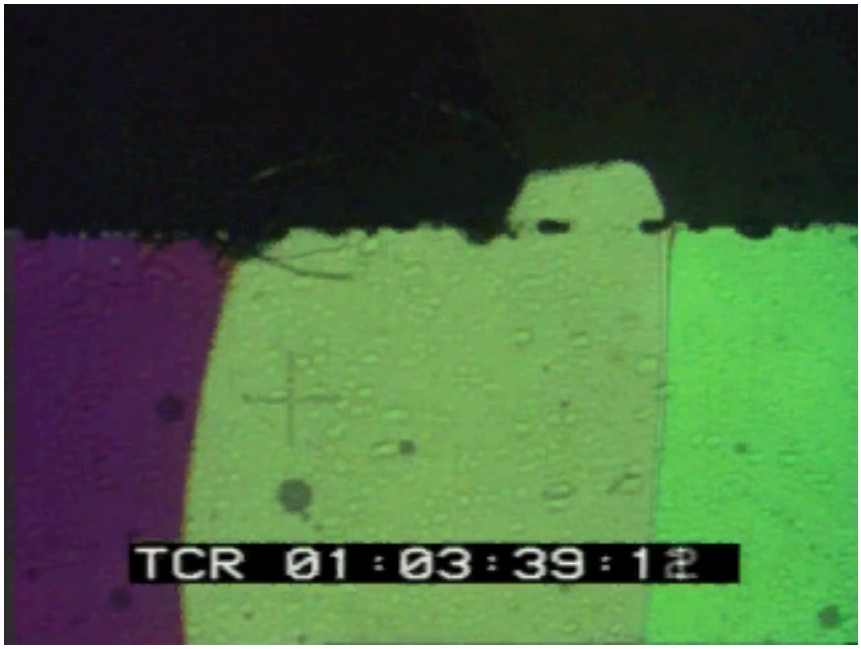

Movie 3 - A pure shear deformation of four ice grains over ≈ 2.5 days.

Click on the image to see the movie. It takes a few minutes to download. So please be patient.

- Grains in hard-glide orientations in combination with nearest neighbour interactions produces a local rotation of the crystal lattice to form kink bands.
- Slip-planes are activated and differently oriented in adjacent grains. As deformation proceeds the slip-planes are bent and this produces undulose extinction and differences in the birefringence colours.
- Intragranular microstructures are well developed, they include undulatory extinction (smooth slip-plane bending), subgrains, kink structures, elongate older grains and the nucleation of recrystallised grains.
- These processes are occurring under dynamic conditions to produce syn-tectonic (or dynamic) recrystallisation. New grain nucleation and grain growth occurs adjacent to and on the boundaries between neighbouring grains. As a result the original grains are reduced in size and preserved as relics between the unstrained new grains.

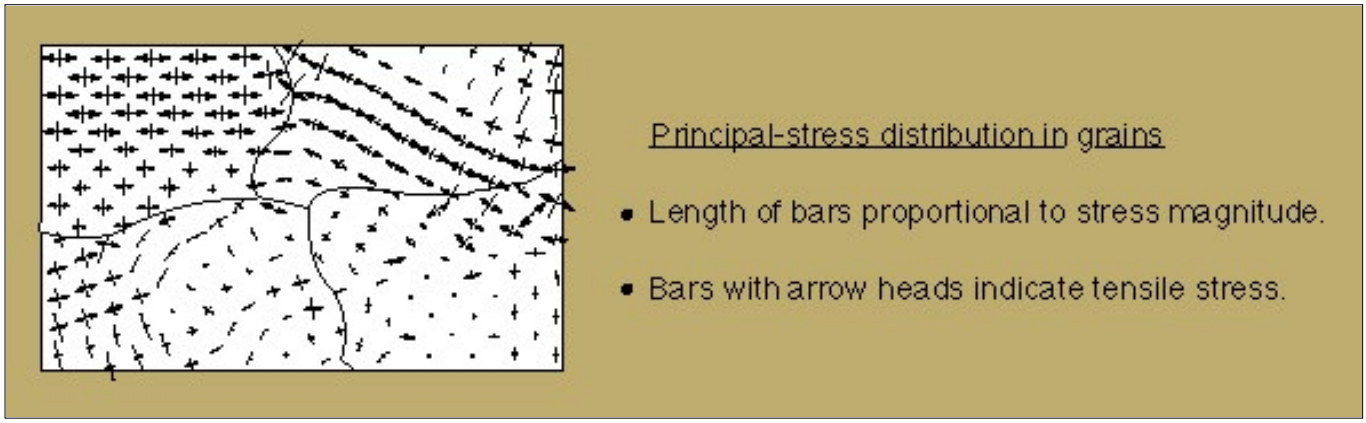

Figure 1.2.4: Numerically generated principal-stress distribution in sample shown in Fig. 1.2.2 and shortened 20% in Fig. 1.2.3 (after Wilson & Zhang 1994).

The Numerical specimen generated in Figure 1.2.4 is from a FLAC (Fast Lagrangian Analysis of Continua) model described by Wilson & Zhang (1994, 1996) and reproduces portion of the coarser-grained ice sample shown in Movie 2. Grains with easy-glide lattice orientations or with lattice orientations favourable for kinking usually show large strains and small stresses (Fig. 1.2.4). Furthermore, grain boundaries, in particular triple junctions, are generally the places where strain and stress are locally strengthened or sharply changed. This is because these areas involve the strongest grain interaction arising from the need to achieve strain compatibility and are the regions where new grain nucleation occurs.

Polycrystalline materials tend to develop a bulk crystallographic preferred orientation in response to its stress, strain rate and temperature history. In the movie below we consider a two-dimensional hexagonal-grain model with grains with variable slip-plane traces that is subjected to axial shortening.

Upon deformation, intragranular slip accommodates most of the deformation and the initial equi-axed grain geometry has been deformed into non-equi-axed shapes. The grains showing high strain are mostly those with deformation-favourable easy-glide orientations. Such deformation can also be represented on deformation maps.

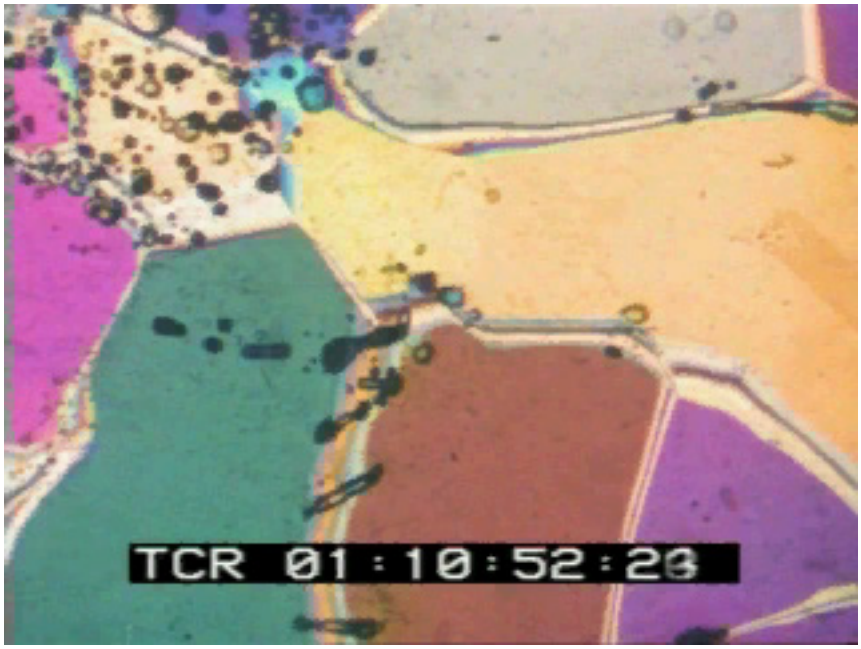

Movie 4 - Polycrystalline ice aggregate deformed in pure shear over ≈ 5 days.

Click on the image to see the movie. It takes a few minutes to download. So please be patient.

- In the pure shear deformation that is seen in movie 4, the sample is shortened 30%.
- Adjacent grains in the initial aggregate have a random distribution of their *c*-axes, when plotted on the lower hemisphere of a stereographic net.
- Slip-lines are developed at different times in adjacent grains.
- As deformation proceeds the slip lines and hence the crystal structure is bent and this produces undulose extinction, as seen in the change in the birefringence colour.
- Grains in a hard glide orientation also develop distinct kink bands.

1.3 Dynamic recrystallisation

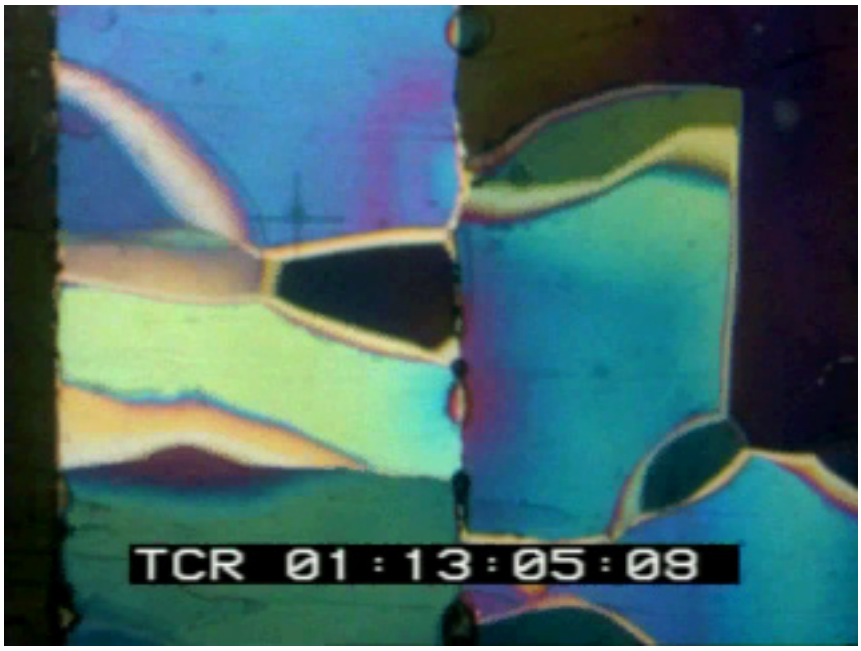

Movie 5 - Polycrystalline ice aggregate deformed in pure shear over ≈ 2.5 days.

Click on the image to see the movie. It takes a few minutes to download. So please be patient.

- With the movement of dislocations on glide planes and the development of the kink bands there is also dynamic recrystallisation.
- Recrystallisation involves new grain nucleation and grain growth.
- Recrystallisation can also reduce the original average grain size leaving behind a few relict deformed old grains (Grain size reduction).

- New recrystallised grains are nucleated as small equiaxed grains and grain boundaries then begin to bulge and migrate as they undergo grain growth.
- These new grains are themselves deformed with the continuing deformation.

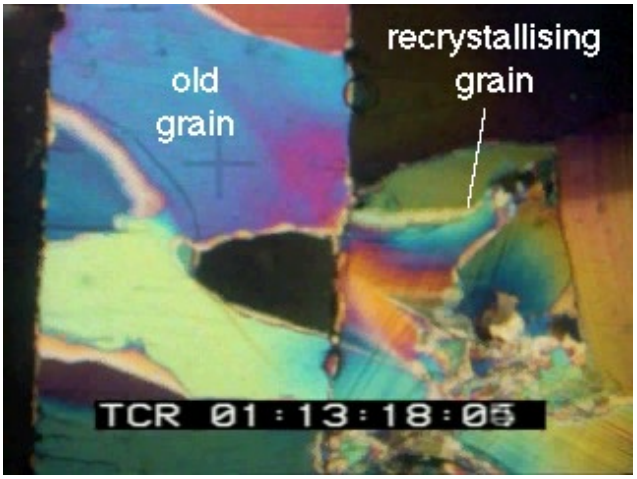

1.4 Grain shape and preferred orientation change

- The pure shear deformation seen in the movies produces a sub-horizontal foliation defined by an alignment of grain shapes.
- Many of the original grains, both in the movies and in the FLAC model below that displayed higher order birefringence colours have disappeared. This reflects the development of a more permissive preferred-orientation within the sample and the evolution of a new fabric.

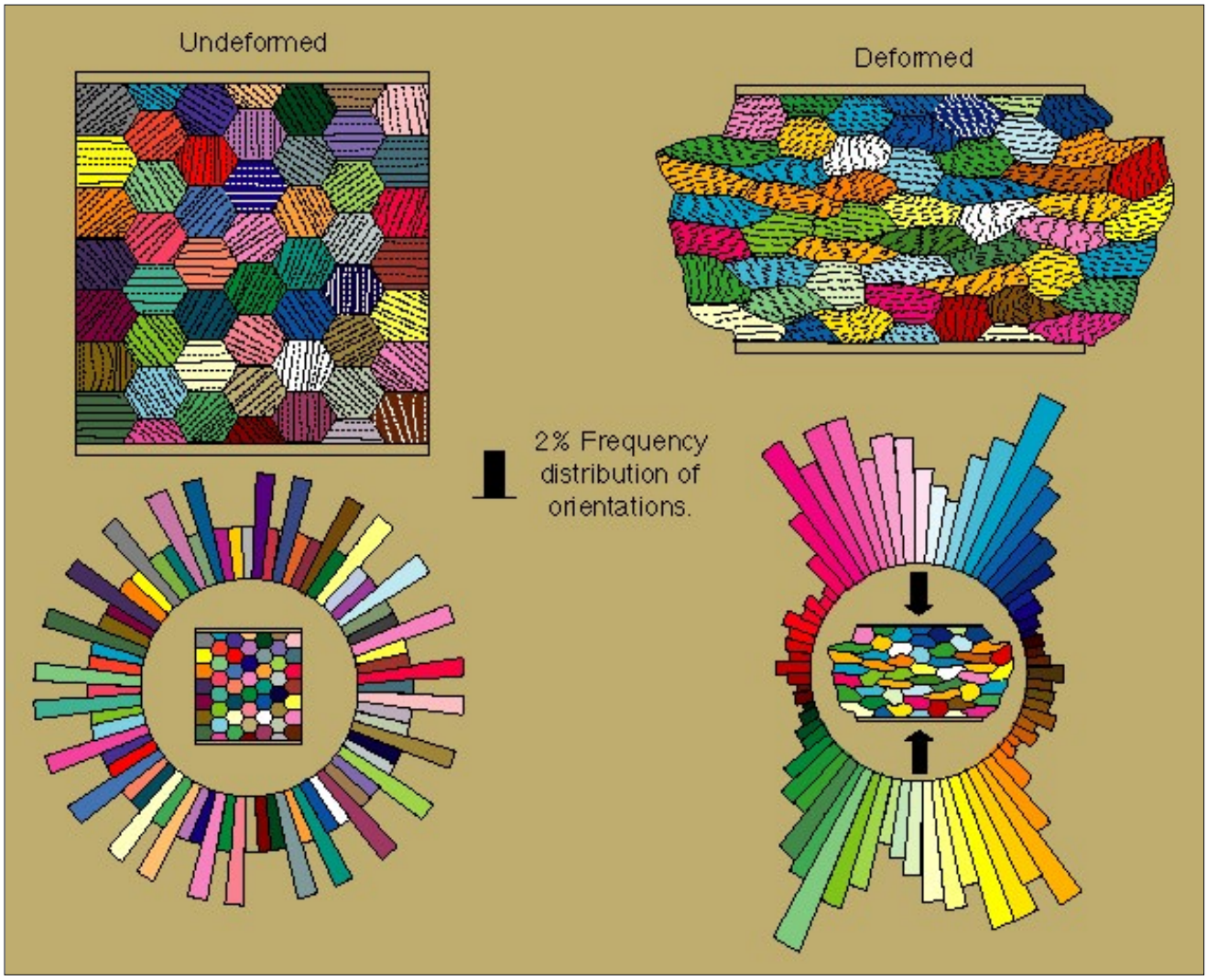

Figure 1.4.1: Polycrystalline aggregate showing: ***Undeformed*** shape of grains and slip-plane traces and initial random two-dimensional orientation of slip-plane normal (*c*-axes) with respect to the specimen orientation. ***Deformed*** by 29% shortening, the grains in the aggregate show elongation parallel to the extension direction and the *c*-axes are concentrated in a bi-symmetrical pattern about the shortening axis. This 2D FLAC model is taken from Wilson & Zhang (1996).

- A two-dimensional view of **Undeformed** grains in a polycrystalline aggregate and slip-plane traces and initial random orientation of slip-plane normal (*c*-axes).
- **Deformed** aggregate shows grain-shape alignment parallel to the extension direction and the *c*-axes are concentrated in a bi-symmetrical pattern about the shortening axis.

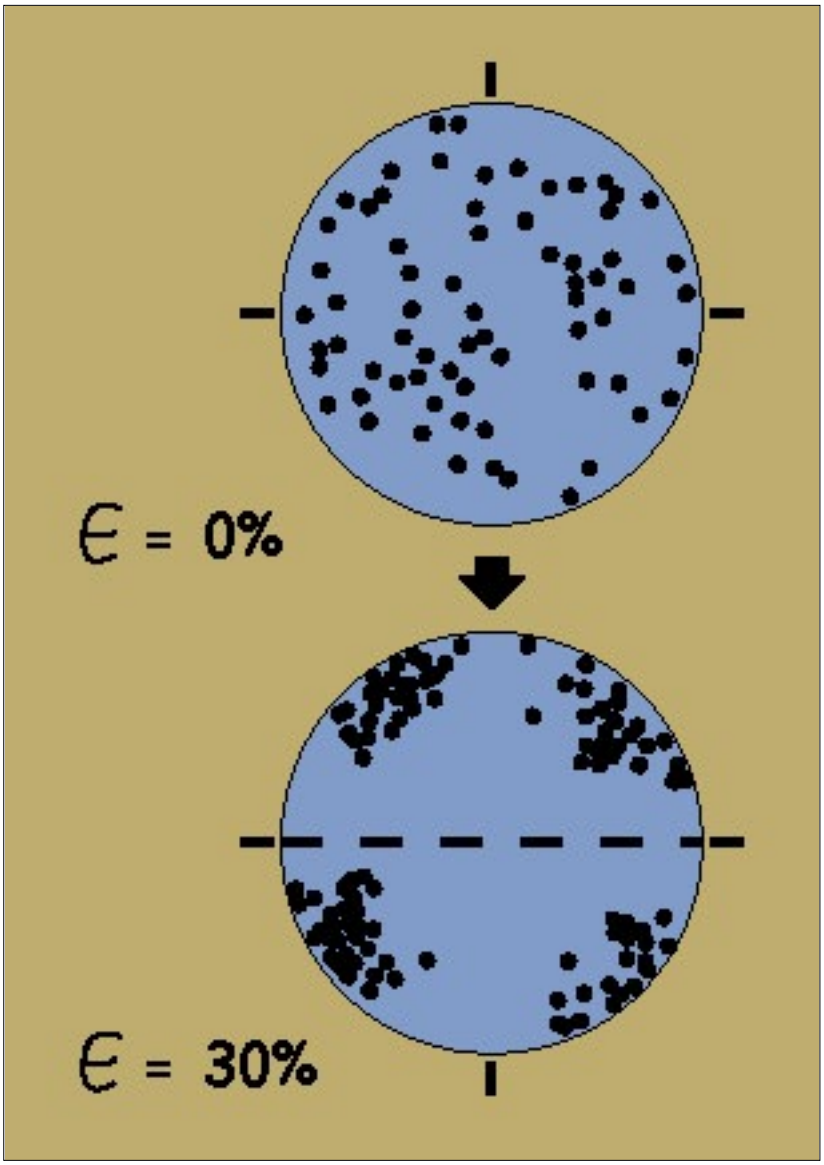

Figure 1.4.2: Stereographic projections that contrast the random *c*-axis preferred-orientation in undeformed verses strong fabric in deformed sample. The broken line represents the grain-shape orientation and hence foliation in the sample.

- Three-dimensional change from randomly oriented *c*-axes in undeformed aggregate (Fig. 1.4.2) to a distribution containing two concentrations of *c*-axes symmetrically distributed about the foliation plane.
- These concentrations are symmetrically related to the shortening axis and the plane of flattening defined by the grain-shape distribution.
- In this pure-shear environment we have the situation where the principal axes of the strain ellipsoid do not rotate.
- The plane of flattening in the corresponding strain ellipsoid will coincide with the alignment of grain-shapes.
- The *c*-axis fabric development is symmetrically related to the shortening

direction.

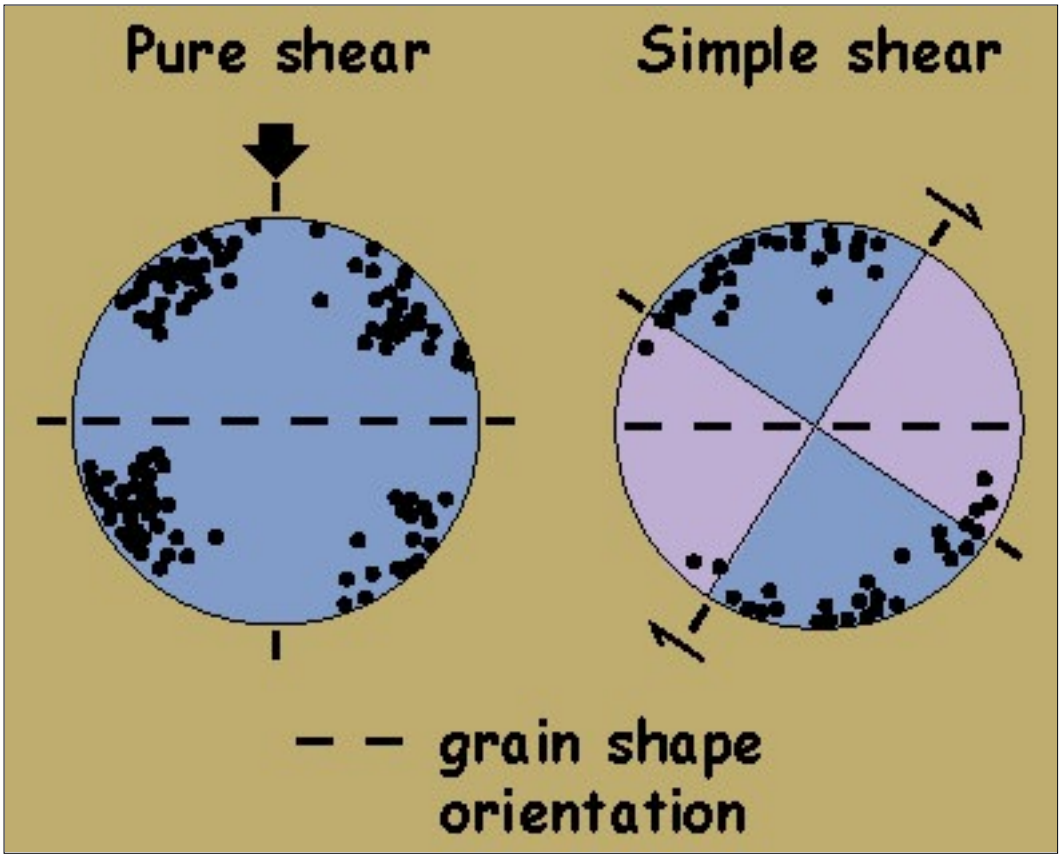

Figure 1.4.3: The *c*-axis distributions in pure shear versus a simple shear regime.

1.5 Fabric

When a stress is applied to a polycrystalline aggregate of ice with a random distribution of *c*-axes, greater than 90% of the deformation is accommodated by glide on basal planes (Castelnau et al. 1996). The deformation of any individual grains is restricted by the glide in neighbouring grains (Fig. 1.2.4). Grains rotate relative to each other and the applied stress so that deformation can proceed. The rotation may be accommodated by grain boundary sliding (Goldsby & Kohlstedt 1997) at the same time as internal glide proceeds. Grains tend to rotate such that their *c*-axes move towards a compressive stress and away from a tensile stress. Thus, ice which has undergone prolonged compression will have *c*-axes oriented in a solid cone about the compression direction (Fig. 1.4.2), while ice that has experienced prolonged tension will have *c*-axes oriented in a girdle orthogonal to the tensile direction. The rotation of grains relative to an applied stress, combined with elongation of grains parallel to their basal planes, produces a mechanical anisotropy and in simple shear this is a strong concentration symmetrically related to the new grain shape fabric (Fig. 1.4.3).

Recrystallisation also contributes to fabric development. If strain is sufficiently high then recrystallisation tends to replace grains at 45° to the compressive direction. Wilson & Russell-Head (1982) and Castelnau et al. (1996) suggest that recrystallisation begins with less than 1% shortening. Once new grains are formed their *c*-axes continuously rotate towards the compression direction leading to a smaller diameter girdle around the compressive axis. If recrystallisation occurs at lower strain then the girdle is thinner and the diameter larger (Van der Veen & Whillans 1994).

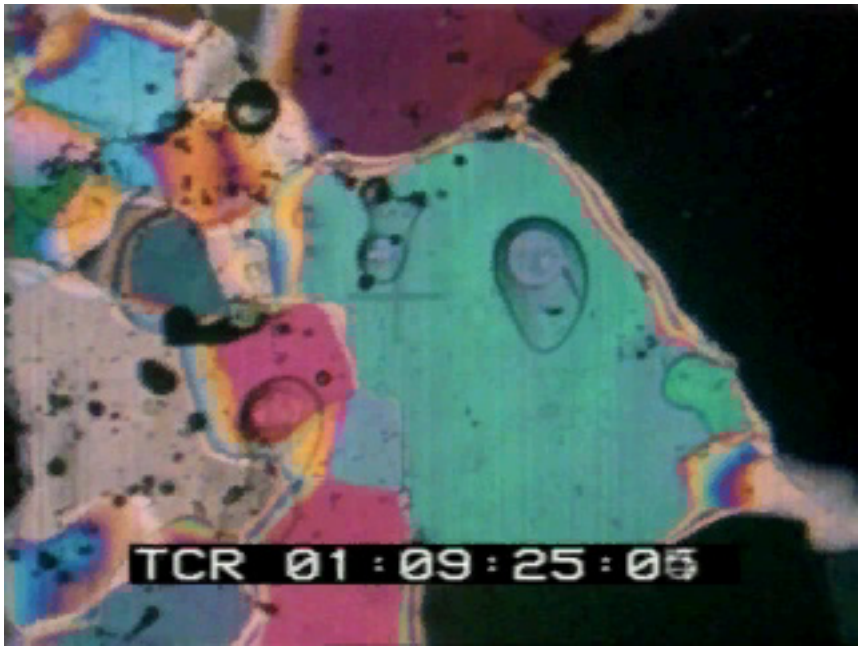

Movie 6a - Polycrystalline ice aggregate deformed in simple shear over ≈ 2.5 days.

Click on the image to see the movie. It takes a few minutes to download. So please be patient.

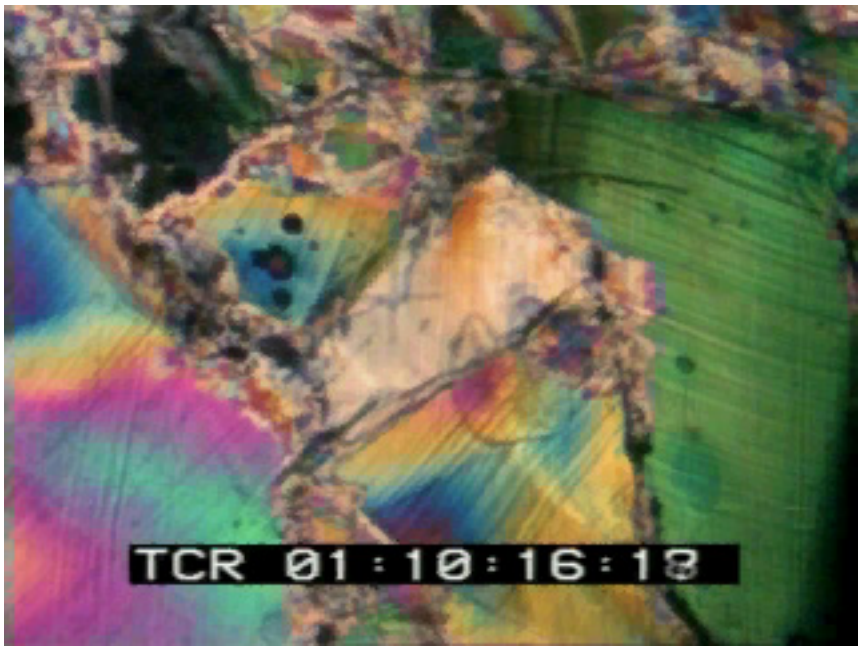

- Ice deforming at -10°C. This is at a lower temperature than the preceding movies where deformation occurred at -1°C.
- It can be seen that the older grains are progressively flattened and rotated during deformation and are part of a foliation forming element.
- Recrystallisation and nucleation during the deformation produces strain-free grains which are not foliation-forming elements until they are deformed.
- The new grain nucleation has the function of destroying, in part, any grain alignment produced during the rotation of the earlier grain population.
- The grain shape is controlled by the rate of boundary migration in a specific direction, that is before grain

Movie 6b - Deformation continued for a further 2.5 days. See sample SS11 described by Wilson & Zhang (1994).

Click on the image to see the movie. It takes a few minutes to download. So please be patient.

growth is arrested by interaction with neighbouring grains with stable crystallographic preferred orientations.

Temperature variation in an ice mass has direct ramifications on strain rate as diffusion flow, basal glide controlled creep and the importance of grain boundary melting and grain growth are temperature dependent. Similarly deformation can be partitioned into two competing regions: (**1**) those where strain softening processes occur by dynamic recrystallisation and (**2**) hard spots or older grains that are undergoing little deformation. Hence as the stress regime and magnitude varies in a glacier, the relative pervasiveness and style of fabrics also varies spatially and temporally. The development of fabric controls strain rate, producing a feed-back loop which further complicates ice flow models and our understanding of plastic deformation.

1.6 Evolution of glacial ice during deformation

Numerical stress maps derived from deformation experiments (Fig. 1.2.4), and the use of such relations to plot deformation mechanism maps, assume that ice is homogeneous and mechanically isotropic. However, an initially isotropic polycrystalline aggregate will develop a fabric after prolonged deformations. In addition to basal glide, deformation is generally accompanied by grain boundary migration, recrystallisation and rotation of crystals (Fig. 1.1.3). All these contribute to a dynamic recrystallisation processes where there is a change in the mechanical properties of a deforming polycrystalline aggregate with time. These processes produce strong mechanical anisotropies in polycrystalline ice and result in the foliation we see in glaciers.

In an ice sheet gravity forces induce internal stresses which drive deformation and glacial flow. Nye (1952) demonstrated that flow is driven by a shear stress acting down the glacier and is related primarily to the surface slope at any point on the sheet and the depth of a column of ice directly below that point according to:

$$\tau = \rho g h \sin \alpha$$ ---------- equation (10)

where α is the surface slope measured from the horizontal, g is accleration due to gravity, h is the depth and ρ is the density of ice. At the base of the glacier the shear stress is assumed to be balanced by friction acting in the opposite direction such that there is no basal sliding. This assumption is true for much of the east Antarctic ice sheet where the ice is generally frozen to its base. Nye (1952) also showed that the shear stress at the base was independent of the slope of the base, so long as the difference in slope between the base and the surface was not large.

Within real ice sheets, the shear stress produced by surface slope is not the only differential stress acting on the ice mass. Changes is surface slope, rapid changes in the bed-rock topography and variations in the accumulation and ablation rates, all produce longitudinal and transverse differential stresses. However, equation 10 can be used to derive a first order estimate of stress conditions in an ice body. For example the surface slope of the section of outlet glacier in the Framnes Mountains, east Antartica investigated by Marmo & Wilson (1998) is ~0.02 Rad and depth of over 800m (Fig. 1.6.1). If equation 10 is applied to this generalised column of ice within this outlet glacier, then the shear stress increases linearly with depth from zero at the surface to 0.17 MPa at a depth of 800m (Fig. 1.6.2).

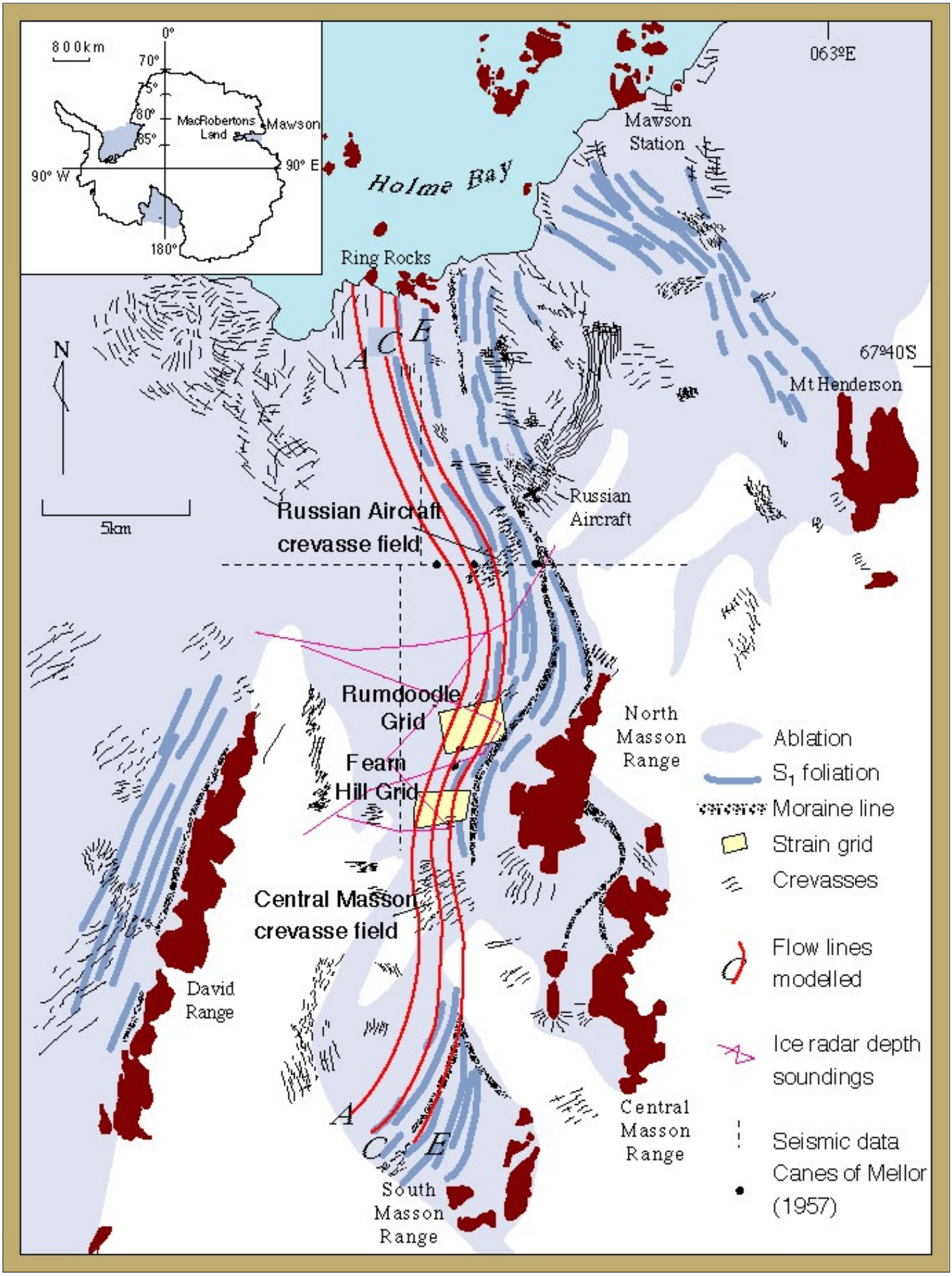

Figure 1.6.1: Flow lines in an outlet glacier in the Framnes Mountains, Antarctica (Marmo & Wilson 1998).

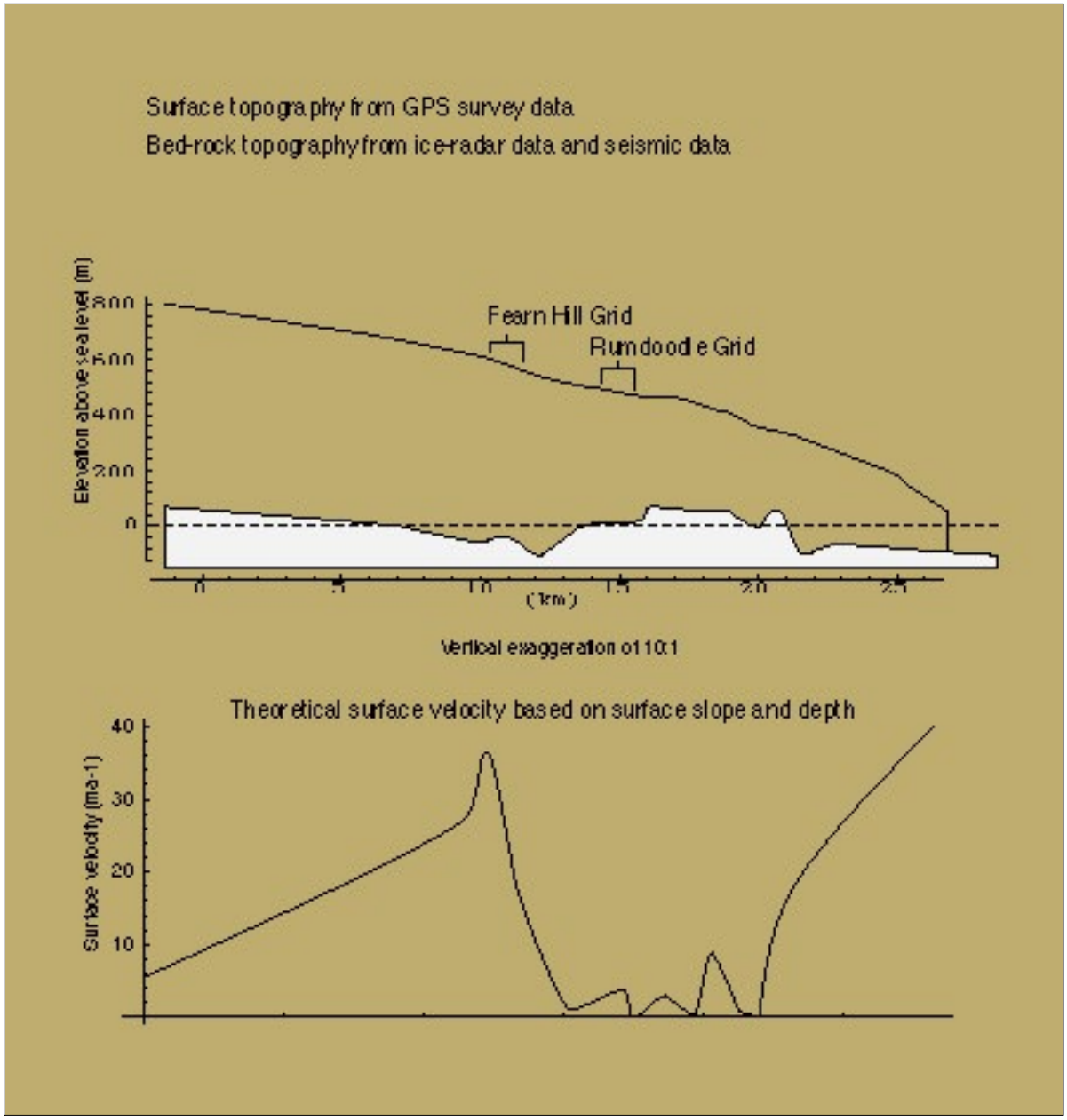

Figure 1.6.2: Longitudinal section parallel to the flow lines in the Framnes Mountains glaciers. The flow lines transect strain grids at Rumdoodle and Fern Hill area where the maximum velocity and bed-rock topography data have been collected.

In a glacier, the orientation and tightness of *c*-axis maxima become dependent on the flow regime (Azuma 1994). In general, the upper part of ice sheets experiences pure shear due to vertical compression and longitudinal extension. If the region is in a parallel flow regime, or a divergent flow regime, the ice experiences progressive uniaxial compression or pure shearing and the *c*-axes rotate to form a broad maximum around the vertical (Fig. 1.6.3). The maximum increases with depth and cumulative strain. If the region is in a convergent flow regime, then longitudinal stresses become important producing progressive uniaxial tension or pure shearing in tension, and a

girdle distribution of *c*-axes orthogonal to the flow direction. The basal ice, and ice close to the margins on the stream, have a strong single maximum due to simple shearing. In outlet glaciers the strain rate is sufficiently high that recovery via dynamic recrystallisation becomes an important process. Recrystallisation tends preferentially to produce new grains at 45° to the compression direction. With continued deformation the *c*-axes of ice crystals rotate towards the compression direction to form a tight girdle in ice at depth. The strong girdle fabric in outlet glaciers tends to produce deformation closer to steady state flow than is observed in other parts of large ice sheets. The flow parameter n=3 (see equation 1) is consistent for most outlet glaciers, except for the uppermost parts where grain growth may still occur reducing n to between 1 and 3 (Alley 1992).

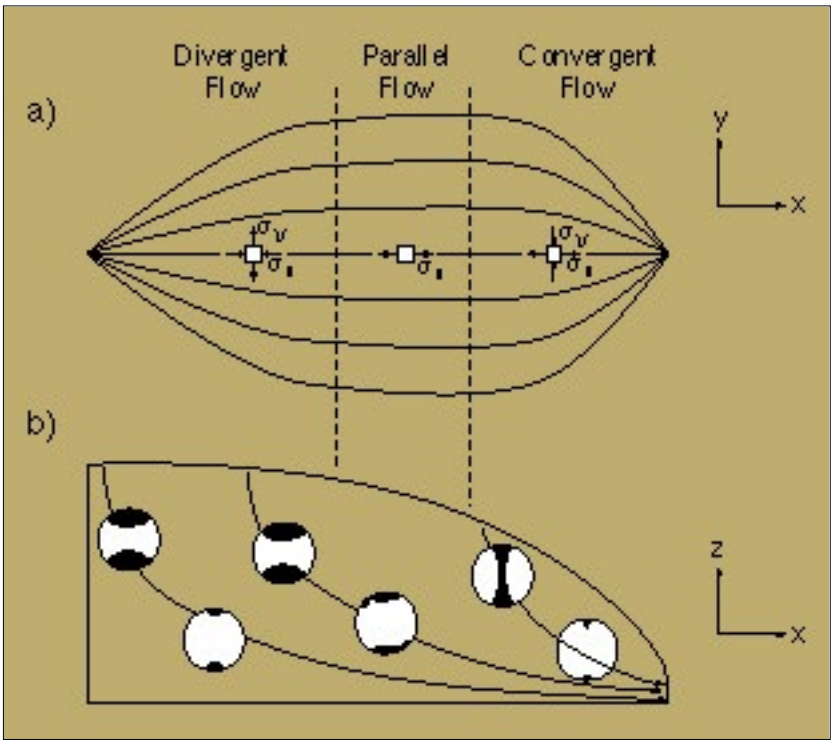

Figure 1.6.3 Divergent, parallel and convergent flow regimes and observed *c*-axes fabric associated with each. (*After Azuma, 1994*)

The development of fabrics can reduce the resistance of the polycrystals to creep for a given applied stress promoting an increase in strain rate. This presents a feedback loop as a strain-rate increase leads to polycrystalline aggregates accumulating more strain, leading to stronger fabrics. It is possible that this process results in bifurcation, as strain is localised into thin layers that are less resistant to glide. Hudleston (1980) noted the development of thin shear zones in the margins of glaciers. The shear zones initially developed as

lenses tens of millimetres thick and attained shear strains greater than $\gamma = 10$. Higher strains were accommodated by the growth and coalescence of these thin shear zones to distribute strain more uniformly through the ice. The continuous development of fabrics and strain localisation adds further complexity to the deformation processes occurring in glaciers and many natural bodies of rock.

Click here for 1.7 REFERENCES

Click here for 1.8 ACKNOWLEDGMENTS

Further information can be obtained from:

C.J.L. Wilson

School of Earth Sciences

The University of Melbourne

Victoria 3010, Australia

Phone: (61) 3 8344 6538

Fax: (61) 3 8344 7761

Email: c.wilson@earthsci.unimelb.edu.au

FLOW IN POLYCRYSTALLINE ICE

Part 2 - Background information

By Chris Wilson and Brett Marmo

2.2 Glaciers

Discharge of ice from the Antarctic and Greenland ice sheets or valley glaciers (Kamb 1959) is controlled primarily by rapid moving ice streams and outlet glaciers. The evolution of glacial ice produces mechanical heterogeneities that change the way an ice mass responds to applied stresses and temperature variations. In order to understand the way a glacier responds to varied stress, strain and temperature histories, it is first necessary to examine the behaviour of ice as a material. In general, deformation in both single crystals and polycrystals is described by *Glen's Law*, where the strain rate, $\dot{\varepsilon}$, is related to stress by a power law of the form:

$$\dot{\varepsilon} = A\sigma^{n} \qquad \text{---------- equation (1)}$$

A and *n* are constants (Glen 1955). However, Glen's empirical flow law does not consider the strong plastic anisotropy due to easy glide on the basal plane.

A flow law that includes a geometric term is therefore required to model anisotropic flow. An anisotropic flow law has been implemented in a finite difference model to estimate the pervasiveness of fabrics in the Framnes Mountain outlet glaciers.

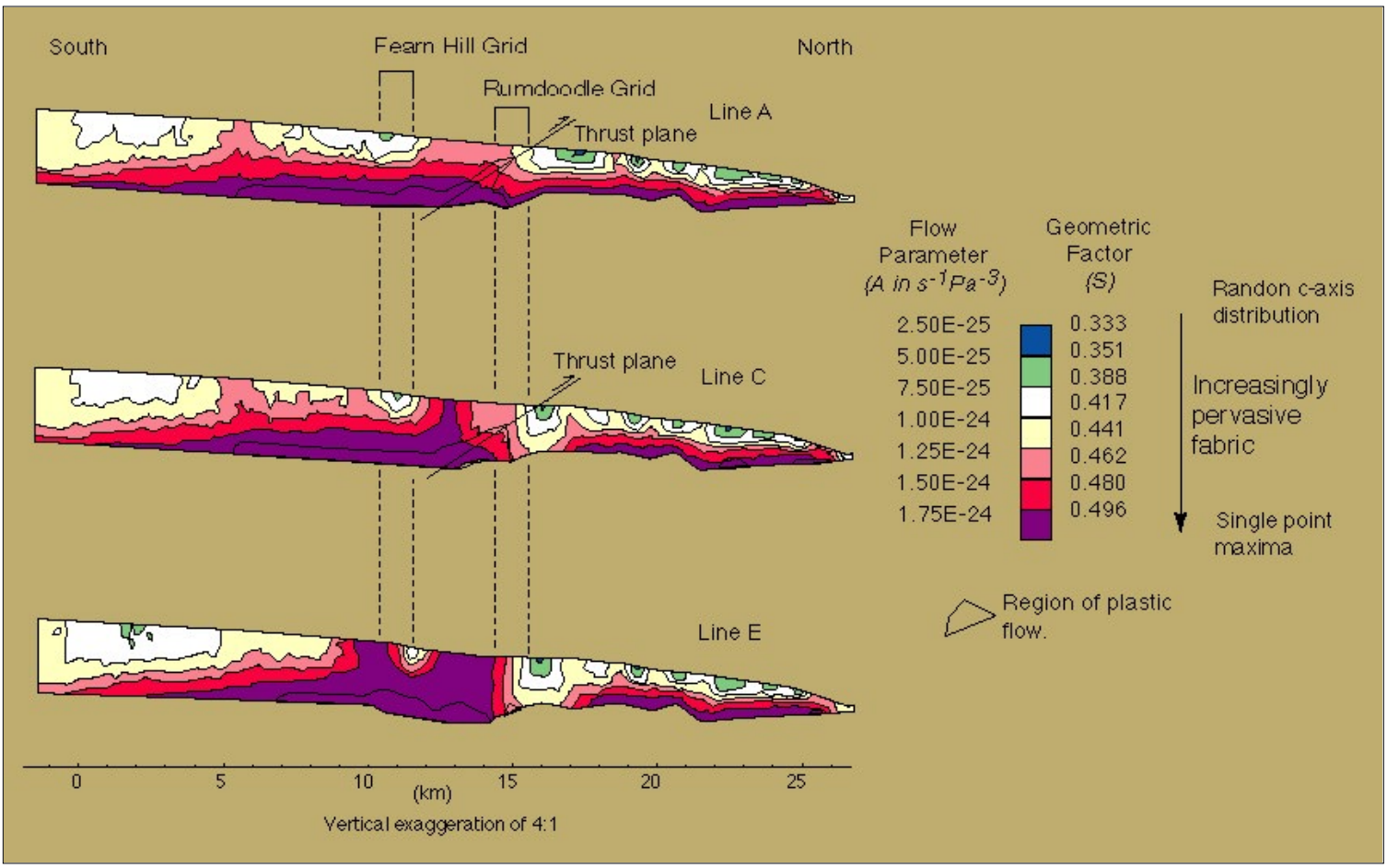

Figure 2.2.1: Simulated fabric development in flow lines from an outlet glacier in the Framnes Mountains, Antarctica (after Marmo & Wilson 1999). The fabric is based on the accumulation of strain over a period of 100 years where the initial *c*-axis distribution was random. The geometric factor that relates the intensity of the fabric is shown, as is the value for the flow parameter *A* that correlates to the geometric term. Areas of plastic flow from visco-plastic models described by Marmo & Wilson (1999) are also shown. Note the development of a thrust plane below the Rumdoodle Grid in Line A.

2.20 Anisotropic flow law for ice

The prolonged deformation of polycrystalline aggregates in glaciers leads to the development of a bulk cystallographic fabric. As a polycrystalline aggregate accumulates strain, the individual crystals rotate by dislocation glide into rotationally stable end orientations. The *c*-axes tend to rotate towards the principal compressive direction and away from the principal tensile direction. Recrystallisation also contributes to the development of the bulk fabric as grains that are poorly oriented for basal glide inhibit those that are more appropriately oriented. The geometric restriction on the movement of dislocations in appropriately oriented grains produces dislocation tangles and a site for the initiation of dynamic recrystallisation (Wilson & Zhang 1994,Wilson 1986). The new grains that are produced by this process tend to form with basal planes at 45° to the compressive direction (see Fig. 1.4.1). Thus, the poorly oriented grains tend to be replaced by grains with the maximum resolved shear stress on their basal planes. The alignment of basal planes to more appropriate orientations for glide leads to strain softening and enhanced flow. Pimienta et al. (1987) report that if an aggregate with a single *c*-axis maximum is deformed by uniaxial or biaxial compression, such that the maximum shear stress is resolved onto the basal planes, then the strain rate is enhanced by 10 times and if the load is applied co-axially with the single *c*-axis maximum, then the strain rate is enhanced by 0.1.

When a fabric develops in an ice aggregate, Glen's Law breaks down as the fabric produces a strong mechanical anisotropy and the strain rate is no longer independent of the orientation of the applied stress. A geometric term based on the mean orientation of *c*-axes in the polycrystalline aggregate must be introduced to equation 1 (Glen's Law), so that the strain rate varies with the orientation of any applied stress. To simplify the approach it is common to assume that single crystals deform by basal glide only (Azuma 1994, Azuma & Goto-Azuma 1996). This method is followed in the example of the implementation of an anisotropic model presented by Marmo & Wilson

(1999).

For the case when glide is assumed to occur on basal systems only, the resolved shear stress on the basal plane of any crystal under uniaxial compression or tension, can be related by a geometric function referred to as the *Schmid Factor*, S_i (Azuma & Higashi 1985):

$$S_i = \cos\phi_0 \sin\phi_0 \qquad \text{---------- equation (11)}$$

where ϕ_0 is the angle between the *c*-axis and the unique stress axis. The Schmid factor for an aggregate as a whole, *S*, is given by the mean distribution of *c*-axes relative to the unique stress axis:

$$\bar{S} = \frac{1}{N_T}\sum_{i=1}^{N_T} S_i \qquad \text{---------- equation (12)}$$

When the *c*-axes are randomly oriented $\bar{S} = \frac{1}{3}$, for pure shear and $\left(\bar{S} = \frac{3}{10}\right)$ for simple shear, and when a fabric is completely developed such that all the *c*-axes are inclined at 45° to the compressive stress axis, $(\bar{S} = 0.5)$. Azuma 1995 showed that the strain on an individual grain was related to the net strain of the aggregate by the ratio:

$$\frac{\epsilon_i}{\bar{\epsilon}} = \frac{S_i}{\bar{S}} \qquad \text{---------- equation (13)}$$

where ϵ_i is the strain of an individual grain and the macroscopic strain of the aggregate is given by $\bar{\epsilon} = \frac{1}{N_T}\sum_{i=1}^{N_T}\epsilon_i$. Azuma (1995) also demonstrated by *in situ* experimental observation, that the strain varies with *S* approximately to the fourth power:

$$\epsilon = 388\bar{S}^{3.7} \qquad \text{---------- equation (14)}$$

The Schmid factor is related to the strain rate by assuming that the stress on any one grain, σ_i, is inversely proportional to the Schmid factor for the grain, and proportional to the Schmid factor for the aggregate as a whole:

$$\sigma_i = \frac{\bar{S}}{S_i}\sigma \qquad \text{---------- equation (15)}$$

where σ is the uniaxial stress on the aggregate. The shear stress resolved onto the base of a single grain, τ_i, is given by:

$$\tau_i = S_i \sigma_i = \bar{S}\sigma$$ ---------- equation (16)

By dividing both sides of equation 13 by time, the strain rate of the aggregate becomes:

$$\dot{\bar{\epsilon}} = \bar{S}\frac{\dot{\epsilon}_i}{S_i}$$ ---------- equation (17)

By substituting Glen's Law and equation 16 into equation 17, a law describing flow of anisotropic ice under uniaxial deformation is arrived at:

$$\dot{\epsilon} = B_0 \bar{S}^{(n+1)} \sigma' \exp\left(\frac{-Q}{kT}\right)$$ ---------- equation (18)

The geometric factor introduced to Glen's Law acts as a scalar quality on the flow parameter *A* $\left(A = B_0 \bar{S}^{(n+1)}\right)$. As *n=3* for polycrystalline ice, the strain rate varies with the fourth power of the Schmid factor. A fully developed fabric $\left(\bar{S} = 0.5\right)$ therefore enhances the strain rate by ~5 times under uniaxial compression, compared to an isotropic aggregate $\bar{S} = \frac{1}{3}$.

FLOW IN POLYCRYSTALLINE ICE

Part 2 - Background information

By Chris Wilson and Brett Marmo

2.1 Time lapse photography

The movie films in this presentation are an acceleration of the actual deformation that is recorded over periods of up to 5 days. The length of an experiment is indicated in the caption of individual movies and a scaling factor can be obtained from the time code superimposed on the movie.

The apparatus (Fig. 2.1.1) used in this presentation permits the in-situ recording of the changes in an ice layer during either progressive simple shear (Fig. 2.1.1) or pure shear (Fig. 2.1.2). A rectangular section of ice 25 x 35 mm and 0.8 mm thick has its lower and upper surfaces confined between two fixed glass plates (Fig. 2.1.1a). The two long edges are constrained to remain parallel by a fixed guide along one, and a sliding plate along the other (Fig. 2.1.1b); the travel of the latter is also constrained by a fixed guide. Displacement is applied laterally to one end by a row of ten moveable platelets pushed by a swinging arm which pivots at one end so as to sweep an arc of ~50° (Fig. 2.1.1b).

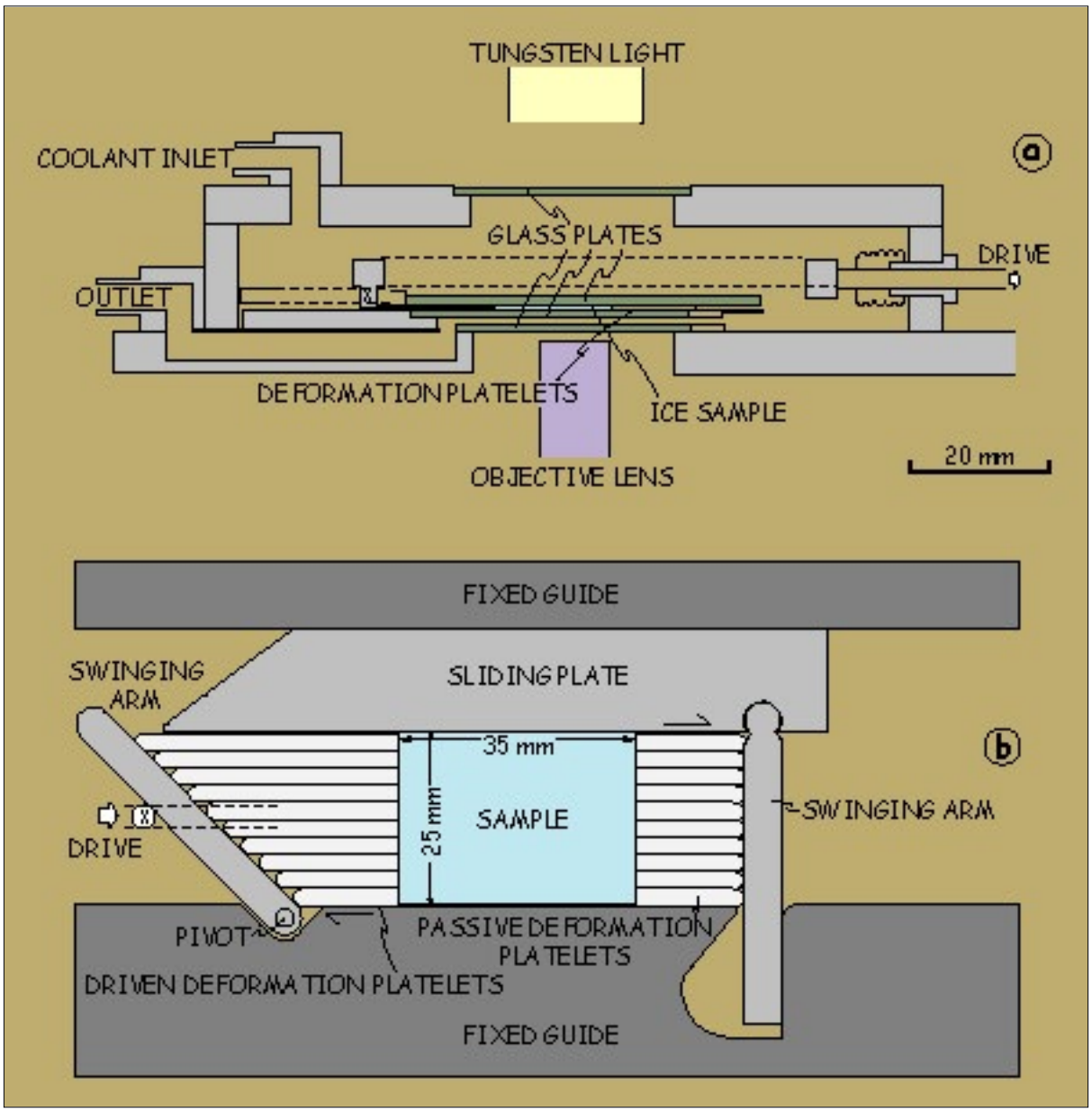

Figure 2.1.1: In-situ simple shear deformation apparatus. **(a)** Section showing location of sample with respect to box containing coolant and the microscope objective lens and light source. **(b)** Plan view of the apparatus at the start of an experiment. At the pivot X the drive moves the swinging arm in a dextral sense.

This arm is driven by a motor which acts through a gearbox and a micrometer. A similar set of platelets at the other end ensures a bulk simple shear of the ice with shear-strain γ ranging up to ~1. The final shape approximates a parallelogram with a step development in the two ends being due to angular terminations of the sliding platelets. While the drive operates at a constant speed and the load is applied parallel to the shear direction.

If a pure shear deformation is applied then two rigid plates at either end of the sample replace the moveable plates (Fig. 2.1.2). One plate is fixed and the other plate is driven against the sample through the same motor gearbox and

micrometer system.

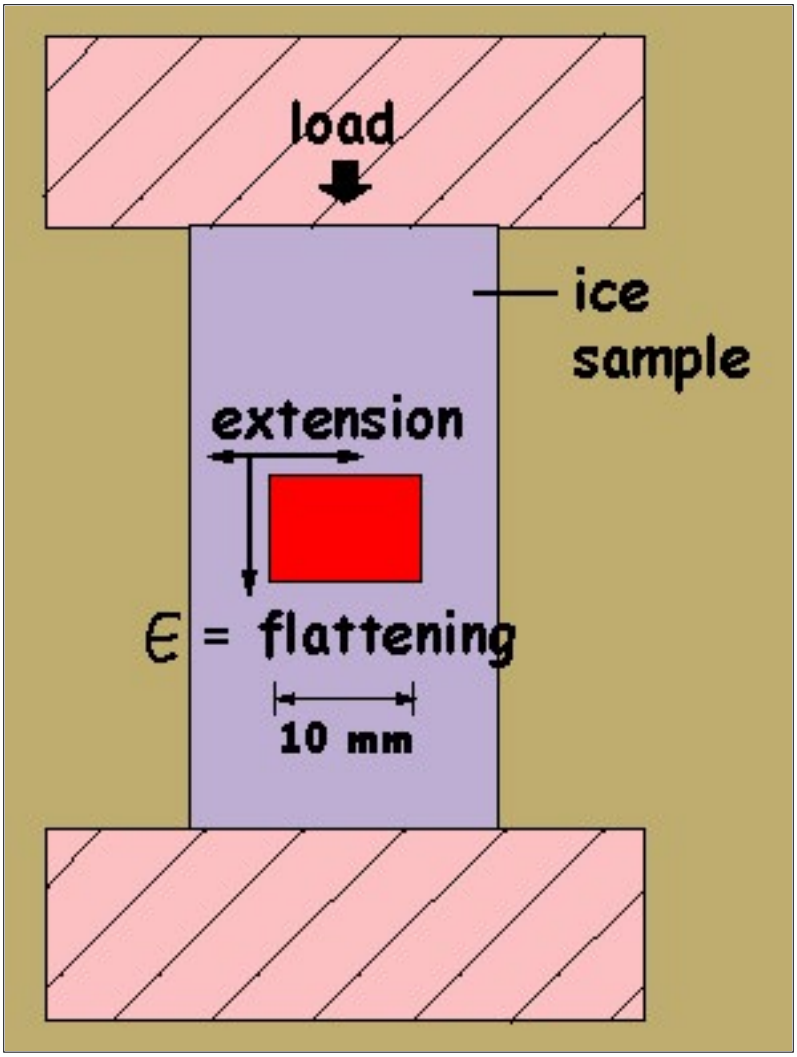

Figure 2.1.2: Plan view of in-situ pure shear deformation apparatus.

The apparatus is enclosed by a sealed box (Fig. 2.1.1a) through which refrigerated silicone oil is pumped to produce a temperature stability of ±0.2°C. The box is then mounted on a Zeiss Invertoscope and microstructural data are recorded from selected areas between crossed polarized light, using a time-lapse system.

The laboratory-made ice used in this investigation was prepared by refreezing a mixture of sieved crushed ice and distilled water [see technical description in Wilson & Russell-Head (1982)]. The samples initially consisted of equant and randomly oriented polygonal grains (mean grain size 2-5 mm) with small (0.1-0.2 mm) spherical air bubbles. The 'artificial' ice was therefore statistically isotropic and measurements showed that it did not display a preferred crystallographic orientation.

FLOW IN POLYCRYSTALLINE ICE

Part 2 - Background information

By Chris Wilson and Brett Marmo

2.3 Dislocations

The mechanical properties of ice are controlled by the presence and movement of dislocations. The movement of dislocations allows ice crystals to deform under applied stresses. In ice , dislocations move on the (0001) plane and in the $<11\bar{2}0>$ and equivalent directions allowing isotropic slip on the basal plane (Fig. 2.3.1). Within the ice lattice there are two sets of basal planes; the shuffle plane, or *S-plane*, and the glide plane, or *G-plane* (Whitworth 1978) (Fig. 2.3.1).

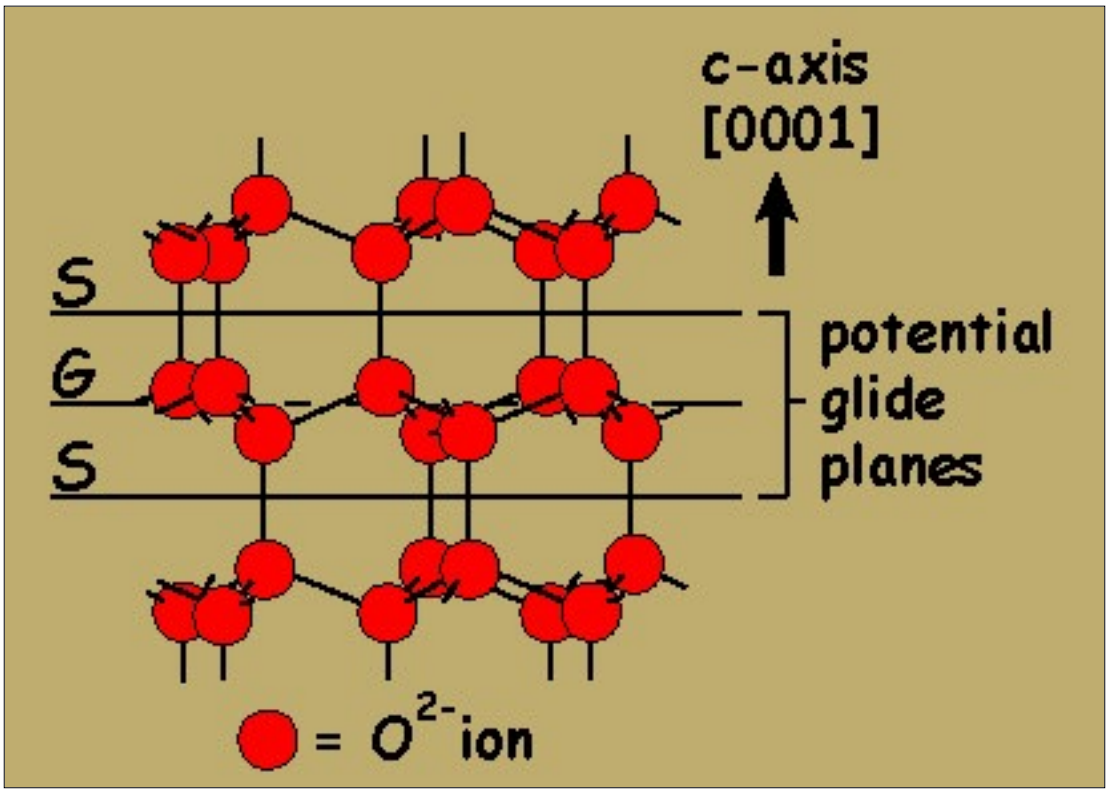

Figure 2.3.1: The crystal structure of ice Ih, showing the arrangement of molecules projected onto the $(10\bar{1}0)$ plane.

The propagation of dislocations results in the re-arrangement of protons (Glen 1968). When a dislocation moves along a slip plane, material above the plane

moves relative to the material below by an amount equal to the Burgers vector. This movement does not affect the arrangement of oxygen atoms as they remain in tetrahedral coordination with the surrounding oxygens. However, the dislocation increases the disorder of the hydrogen atoms (Fig. 2.3.2). The disorder of protons is an infringement of the Bernal-Fowler rule. This disorder of protons is referred to as a Bjerrum defect (Bjerrum 1951), and is specific to the ice structure. As the dislocation propagates it creates a pair of Bjerrum defects: L-defects, which are bonds with no protons; and D-defect, which are bonds with two protons (Fig. 2.3.2).

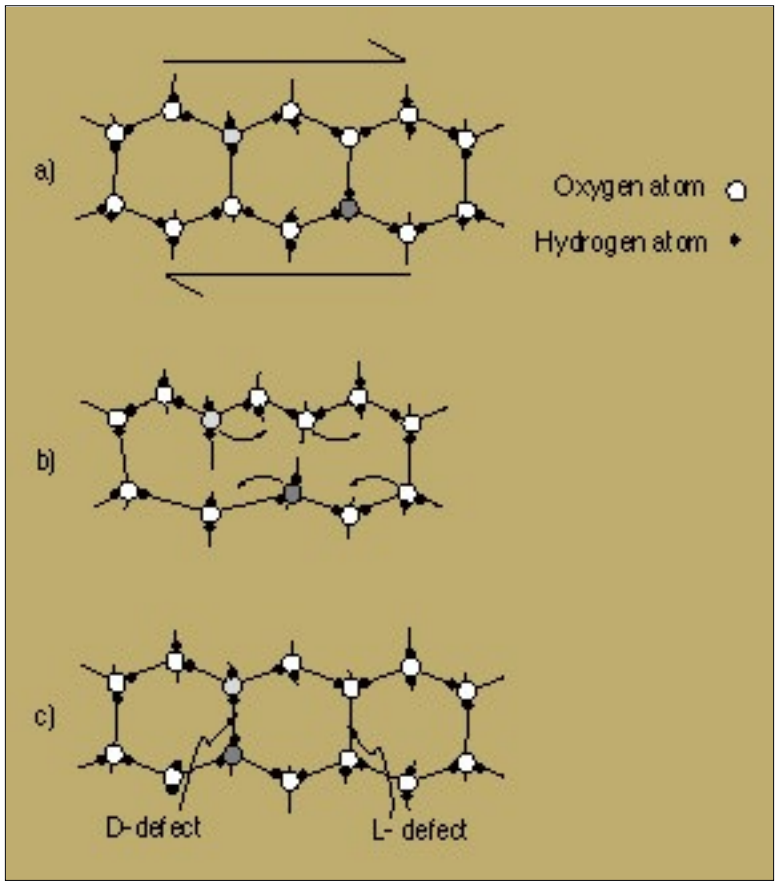

Figure 2.3.2: The propagation of a dislocation through the basal plane of an ice lattice. Oxygen atoms remain in tetrahedral co-ordination after the dislocations have passed. However, Bjerrum defects are produced by the passage of a dislocation leading to disordering in the co-ordination of the hydrogen atoms. L-defects are produced if the inter-molecular bonds contain no protons, and D-defects are produced if the bonds contain two protons (Adapted from Poirier, 1985).

Another possible re-arrangement of protons that avoids the creation of Bjerrum defects will occur if the hydrogen atom crosses the bond and joins the neighbouring oxygen before the dislocation disconnects the bond. This will result in the creation of a $(H_3O)^+$ cation and a $(OH)^-$ anion. The energy required to create a pair of ionisation defects is greater than that required for a Bjerrum defect so that ionisation defects are less likely to be created.

The yield stress observed in shear experiments is more than three orders of magnitude less than the theoretical value. An explanation for this may be the migration of Bjerrum defects through the lattice (Glen 1968). Goodman et al. (1981) considered the way proton rearrangement controls the drift velocity of a dislocation propagating through the lattice as a pair of kinks. Kink pairs nucleate at sites adjacent to areas where no proton rearrangement is required. A kink is held up at any point where a pair of defects is needed to be created to break the bond between molecules. Re-orientation of the protons by migrating point defects allows the dislocation to continue its journey.

Dislocation motion studies using *in situ* experiments have been performed by Ahmad et al. (1986) and Shearwood & Whitworth (1991) using a synchrotron X-radiation technique. Single crystals of ice where mounted in a compression jig and loads, up to 65 N, were applied at ~23° to the basal plane. The loads were applied between 20s and 180s then an X-ray defraction topograph was taken. The stress was then re-applied and another topograph exposed. A series of topographs were taken in this manner and the evolution of dislocation loops recorded. Dislocations with 60° orientations and screw dislocations were recognised in the basal planes of the deformed samples.

This is similar to the observations of Jia et al. (1996) and Liu et al. (1995) who also employed dynamic *in situ* x-ray topographic deformation studies. They were able to show that the basal slip system with the highest Schmid factor was found to be the most active in polycrystalline ice. Whereas, grain boundaries act both as effective sources of lattice dislocations and as strong obstacles to dislocation motion. To act as a source the basal slip is transmitted through a grain boundary, i.e. dislocation impingement on one side of a grain boundary leads to dislocations being emitted from the other side of the grain boundary.

Dynamical straining experiments (Shearwood & Whitworth 1991) of stressed single crystals of ice have determined the velocity of dislocation motion

increased linearly with stress; for crystals between -4°C and -39°C. The velocity of screw dislocations for any stress resolved on to the basal plane, at -20°C is $0.8\,\mu ms^{-1}MPa^{-1}$ with an activation energy for motion of 0.95±0.05 eV. The 60° dislocations has a velocity of $1.6\,\mu ms^{-1}MPa^{-1}$ for any stress resolved on to the basal plane, with an activation energy of 0.87±0.04 eV. However, *in situ* straining of polycrystalline ice has shown that grain boundary regions always deform before the grain interiors (Baker 1997). Where dislocations are emitted in order to accommodate grain boundary sliding this leads to stress concentrations at the grain boundary facets. Eventually, the dislocations which have been emitted traverse the grain and pile-up at the opposite grain boundary-and lead to nucleation of new recrystallised grains.

By Chris Wilson and Brett Marmo

2.5 Generation of defect structures

Dislocations in ice are initiated at Frank-Read sources (Weertman & Weertman 1964). Frank-Read sources occur when a dislocation is pinned at two points within the crystal lattice. The dislocation may be pinned by impurities or it may be a dislocation loop that lies oblique to the basal plane and so is immobile. In the latter case, the section intersecting the basal plane can be considered as a line dislocation pinned at its ends by the immobile sections that are oblique to the basal plane (Fig. 2.5.1). When a small stress is applied to the lattice the pinned dislocation bows. With increasing stress the bow becomes unstable and grows to form the shape illustrated in figure 2.5.1d. The dislocation becomes unstable if the shear stress $\tau \geq Gb/l$, where G is the shear modulus of ice, b the Burgers vector, and l the length of the Frank-Read source. With continued stress the loop grows and eventually curls onto itself (Fig. 2.5.1e). Where the loop touches itself, the dislocations have opposite signs and so obliterate each other, leaving a complete dislocation loop and a dislocation line pinned in the original position. The dislocation loop is now able to propagate through the lattice, while the pinned section goes onto initiate further dislocations. Ahmad et al. (1986) observed multiple generations of dislocations from a single Frank-Read source using X-ray diffraction techniques. Their topographs show the development of dislocations in regions of crystals initially free of dislocations. The dislocations were predominantly in screw orientations or 60° to the Burgers vector and on the basal plane. Dislocations in this orientation encounter a Peierls barrier which forces the expanding dislocation loop to take on a hexagonal shape (Ahmad et al. 1992).

Ahmad et al. (1992) proposed a mechanism related to edge dislocations on non-basal planes as a second source for initiating dislocations. If a significant stress is applied to an appropriate prismatic plane, a segment linking two basal planes will begin to glide. The motion of non-basal edge dislocations is high compared to basal edge dislocations. The rapid motion of the non-basal segment generates dislocation loops on many of the basal planes that the

segment passes through. Ahmad et al. (1992) have used X-ray topographs to show a series of dislocation loops in basal planes stacked one upon the other that appear to have been generated in this fashion.

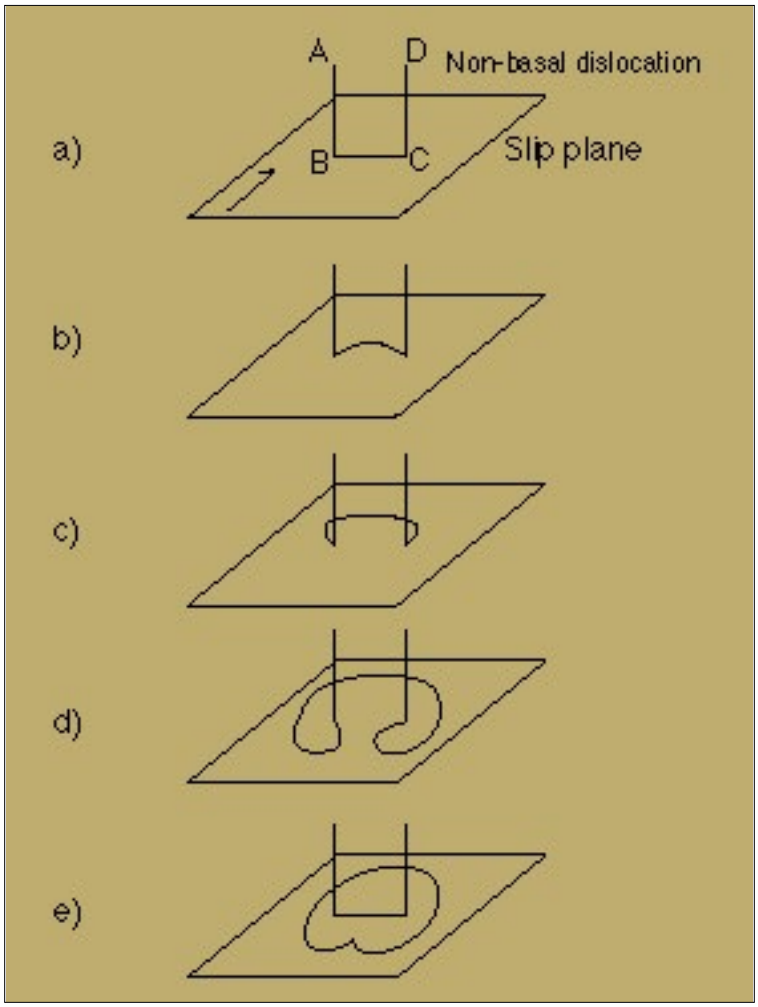

Figure 2.5.1: A Frank-Read source for the multiple initiation of dislocation loops. A dislocation is pinned in the basal plane at two ends by either impurities or an immobile non-basal dislocation. If a shear stress is resolved onto the basal plane, the dislocation line becomes unstable and begins to bow. With increasing stress, the line bows back onto itself to produce a new loop that is free to propagate, and a section that remains pinned which may initiate more loops.

FLOW IN POLYCRYSTALLINE ICE

Part 2 - Background information

By Chris Wilson and Brett Marmo

2.6 Crystal Structure

Ice like other crystalline solids deforms with both an elastic and a plastic component (Petrenko & Whitworth, 1999). If a small amount of stress is applied to ice for a short period of time, the ice will elastically deform. When the stress is removed the ice will return to its initial shape; the strain is completely recoverable. If the stress exceeds a certain amount the ice will be deformed irreversibly. This is *plastic* deformation and the critical stress above which the crystal deforms permanently is known as the *elastic limit*. Ice also will be permanently deformed if stress below the elastic limit is applied for a prolonged period of time. Such time dependent plastic deformation is known as *creep*.

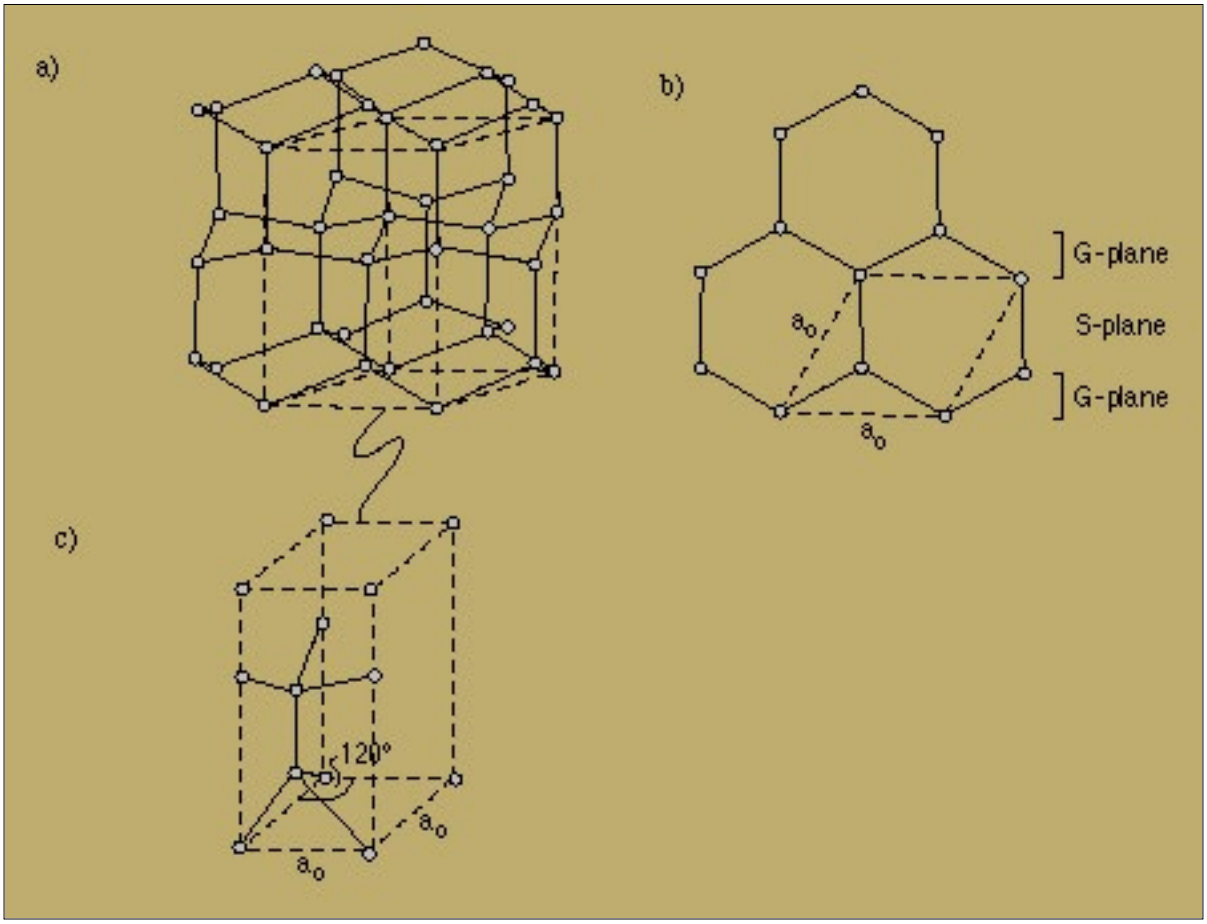

Figure 2.6.1: The Ice Ih lattice. a) Perpendicular to the *c*-axis. The puckered layer of atoms composes

the glide plane, or *g*-plane, and the vertical bonds accommodating hydrogen atoms is the shuffle plane, or *s*-plane. b) Viewed down the *c*-axis, *a* is the unit cell and Burgers vectors parallel this direction (After Hobbs, 1974).

Two mechanisms are known to contribute to creep in ice. The motion of dislocations allows the relative movement of molecular planes within the crystal lattice (Fig. 2.6.1) to permit deformation. This processes in known as *glide*. A second deformation mechanism involves the movement of single ions (Nabarro 1948) or dislocations (Herring 1950) through the volume of a crystal lattice or around the grain boundary (Coble 1963). Diffusional processes act very slowly in ice and are observed when the deformation regime involves very low stresses.

FLOW IN POLYCRYSTALLINE ICE

Part 2 - Background information

By Chris Wilson and Brett Marmo

2.7 Ice

Two solid phases of water are known to occur at the earth's surface. Water molecules that freeze at normal atmospheric condition and between 0°C and -80°C form a crystalline solid, with hexagonal symmetry, referred to as hexagonal ice or Ice Ih (Petrenko & Whitworth, 1999). Ice below -80°C and above -130°C has a cubic symmetry, and so is referred to as cubic ice or Ice Ic. There are a further eight high pressure polymorphs of ice that have been recognised at pressures greater that 200 MPa (Bridgman 1937). Ice within outlet glaciers at the fringes of the Antarctic ice sheet is exclusively hexagonal ice.

Ice *Ih* has a wertzite type structure with layers of oxygen atoms arrayed in puckered hexagonal rings that are stacked in a ABAB sequence (Fig. 2.6.1). The concentration of oxygen atoms in these puckered planes forms the basal plane within the crystal. The *c*-axis of the crystal is perpendicular to the basal plane.

Each oxygen atom must have two hydrogen atoms associated with it. The angle between oxygen atoms within Ice *Ih* is 109°, thus only a small variation of the H-O-H angle in the gas phase is necessary to accommodate hydrogen in the Ice Ih lattice. The hydrogen atoms lie 1Å from their associated oxygen atoms and 1.76Å from the closest neighbouring oxygen atom. There are six possible configurations of hydrogen atoms around oxygen atoms that satisfy this arrangement.

2.8 Basal glide

Ice *Ih* readily undergoes plastic deformation if a component of shear stress acts on the basal plane (McConnell 1891; Kamb 1961). The ease of this style of deformation is due to the slip or glide across the basal plane. Slip along the basal plane is facilitated by the movement of dislocations through the *G*-planes of the lattice. The orientation of the crystal within a stress regime defines how and if the crystal deforms. Nakaya (1958) performed a series of experiments by applying a loaded wedge to the centres of ice crystals that were supported at each end by stationary wedges (Fig. 2.8.1). When the wedge was applied parallel to the basal plane, glide occurs readily and is localised close to the applied stress (Fig. 2.8.1a). When the wedge is applied at 45° to the basal plane, again glide occurred and the crystal bowed (Fig. 2.8.1b). These two orientations are referred to as *easy glide* orientations. When the load was applied (**1**) perpendicular to the basal plane little deformation occurred and the crystal kinked to form a V-shape (Fig. 2.8.1c) and (**2**) perpendicular to the *c*-axis and parallel to the basal plane then negligible deformations occurred (Fig. 2.8.1d). These orientations are referred to as *hard glide* orientations. Little deformation occurred because there was no component of shear stress along the basal plane.

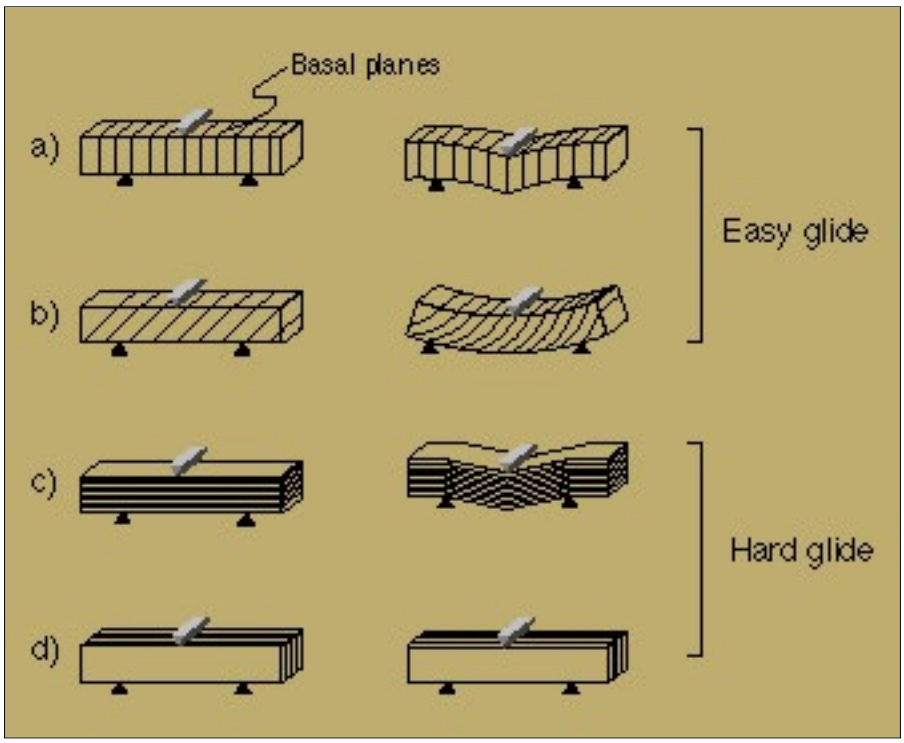

Figure 2.8.1: When a cantilever is applied to a single crystal of ice the deformation style is dependent on the orientation of the basal plane relative to the load. Both a) and b) are in easy glide orientations, such that a shear stress is resolved onto the basal plane. These deform readily when a stress is applied. c) and d) are in hard-glide orientations where no shear stress is resolved onto the basal plane. These are very resistant to deformation.

2.9 Strain rate for glide on basal systems

Ice *Ih* experiences work softening when a shear stress is applied across its basal plane over a prolonged period of time Glen & Perutz (1954), Steinemann (1954), Griggs & Cole (1954), Rigsby (1957). That is, the strain rate increases with time. This process is unusual as most solids work harden during basal glide. Griggs & Cole (1954) applied compressive stress at 45° to the *c*-axis of ice crystals between -10°C and -11°C (Fig. 2.9.1). The creep curves can be described by:

$$\epsilon = \left(0.62\left(\sigma - 0.02\, T_c^2\right)\right)^2 t^{\frac{1}{3}}$$

---------- equation (2)

where ϵ is the compressive strain as a percentage, σ the compressive stress in bars, T_c the temperature in °C below the melting point, and t the time in hours.

Steinemann (1954) applied varied shear stresses to the basal planes of ice crystals. His results showed a slow strain rate for the first 20% of strain (primary strain), then a rapid increase (Fig. 2.9.1). For long periods of time the strain rate eventually becomes constant. At a temperature of -2.3°C the shear strain rate, $\dot{\epsilon}_s$, was related to the shear stress, τ, by:

$$\dot{\epsilon}_s = A\tau^n \qquad \text{---------- equation (3)}$$

where *A* is a temperature dependent constant and *n* is a constant between 1.3 and 1.8 for large strains and 2.3 and 4 for the primary strain.

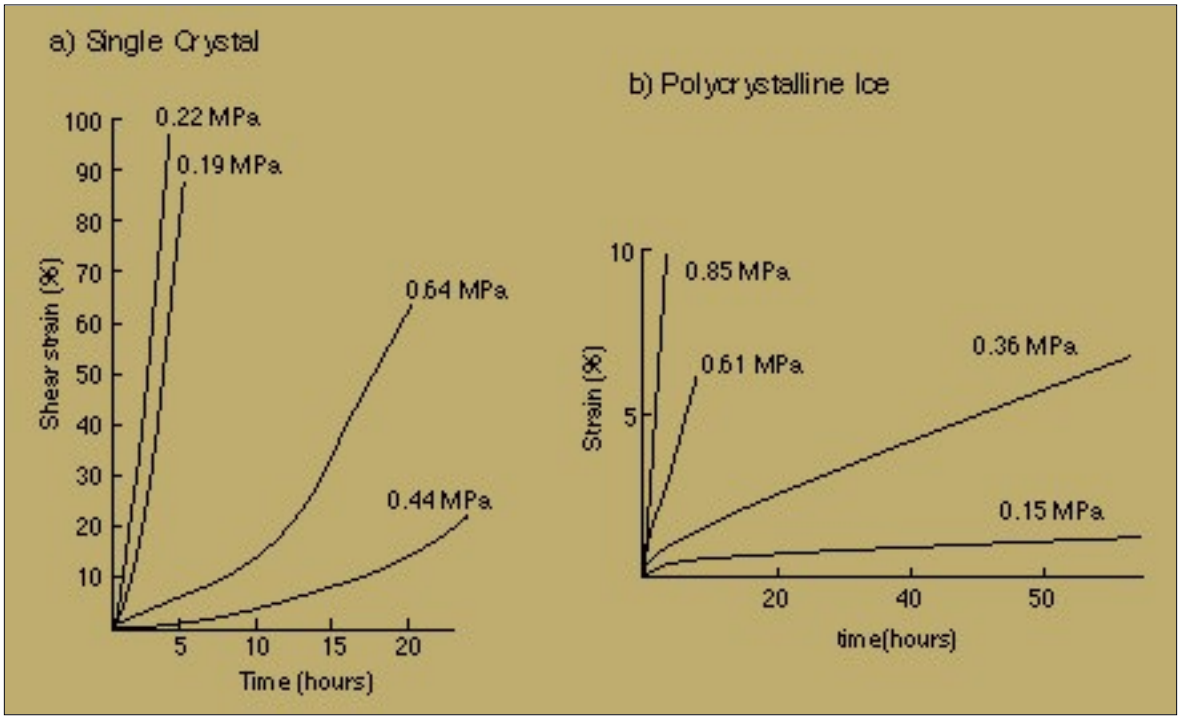

Figure 2.9.1: Creep curves in ice. **a**) The variation in strain in a single crystal under a constant applied stress. Single crystals exhibit strain softening when glide occurs on the basal plane. The strain rate initially increases with time until a constant strain rate is reached (After Griggs and Cole, 1954). **b**) Polycrystalline ice under a constant stress, the initial deformation is rapid, strain hardens, then slows with time until it reaches a constant strain rate (After Glen, 1955).

Wakahama (1962) performed extensive deformation experiments on glacial ice. Tensile and compressive stresses applied to plates of ice at -10°C, where the *c*-axes of crystals were contained within the plane. Stress was applied at between 20° and 45° to the *c*-axis at constant strain rate and a schematic stress-time curve was developed from the experimental results (Fig. 2.8.2). When the shear strain rate was greater that 12% per hour the stress rises quickly from O to A, then drops sharply due to a cleavage fracture occurring on the basal plane. At low strain rates of 3% per hour, the stress followed a curve OBC. At B the yield stress, σ_o , was obtained at which point the ice was able to creep at a constant rate without increasing the shear stress. The magnitude of the yield stress increases with strain rate. Results show that:

$$\dot{\epsilon}_s = 7.3\times10^{-5}(\tau - \tau_{cr})^3$$ ---------- equation (4)

where $\dot{\epsilon}_s$ is the shear strain rate as a percentage per second, τ the shear stress in bars, and τ_{cr} is the critical stress, which is defined as the smallest stress required to initiate slip on the basal plane. The critical stress for ice at -10°C is ~0.02 MPa.

With the strain kept constant after C, the stress relaxed along CD, according to:

$$\frac{1}{\tau} = \frac{1}{\tau_y} + (\text{constant})\,t$$ ---------- equation (5)

where *t* is the time measured from the moment the strain was stopped, τ_y and τ are the shear stress at time 0 and *t* respectively. Relaxation stress was also observed when strain was stopped during the primary deformation (OB). The stress relaxed more slowly if the strain was stopped earlier in the deformation.

Wakahama (1962) assumed that dislocations were initiated and renewed as Frank-Read sources (Fig. 2.5.1). The internal Frank-Read sources lie at different distances from the periphery on the crystal. When a stress is applied to the basal plane, all the sources that have a length that satisfy` $\tau \geq Gb/l$ will begin to create dislocation loops. From theory and observation, when σ, the velocity, v, of a dislocation moving through ice at -10°C is given by:

$$v = [\text{constant}]\sigma$$ ---------- equation (6)

where the constant is $1.043 \times 10^{-10}\ kg^2 m^{-3} s^{-3}$. The maximum stress that the basal plane of ice can withstand without fracturing is ~2 MPa. At 2 MPa across the basal plane, the velocity of a dislocation is $7 \times 10^{-5}\ ms^{-1}$. This is much slower than for other materials such as metals that have a velocity in the order of $1\ ms^{-1}$ (Hobbs 1974). The dislocation loops therefore take some time to reach the surface of the crystal. When the stress is initially applied, the dislocations created from sources close to the surface of the crystal will propagate to the edge first and a small amount of strain will be observed. Over time dislocations created from deeper in the crystal will emerge and their contribution to strain will be summed with those that continue to be created close to the crystal's edge, resulting in an increase in strain rate, hence strain softening. Eventually dislocations formed at the center of the crystal will emerge at the edge so that all the Frank-Read sources appear to be contributing to the strain. From this point on the strain rate will be constant with respect to time.

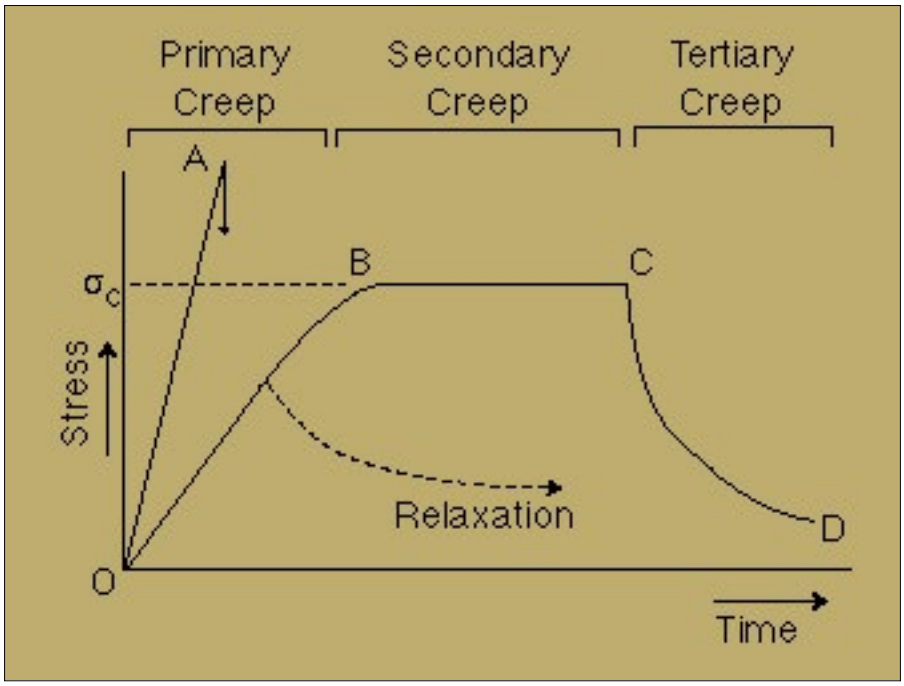

Figure 2.9.2: A schematic sketch of stress-time curve for deformation in a single crystal of ice at -10°C (After Wakahama, 1962).

Weertman (1963) applied steady state motion of visco-elastic materials theory, developed by Schoeck (1956) and Eshelby (1961), to explain creep features in ice. The stress field around a dislocation induces order around the moving dislocation. This reorients protons within the lattice and acts as a viscous drag on the motion of dislocations. If steady state creep is controlled by this mechanism, then the maximum shear strain rate, $\dot{\epsilon}_{ss}$, is given by:

$$\dot{\epsilon}_{ss} = \frac{16\Pi^2}{\Lambda_{max}\,\tau_m G^3}\,\sigma^n$$ ---------- equation (7)

where Λ_{max} is the maximum value of the logarithmic decrement of the internal friction peak, τ_m the average mechanical relaxation time and *G* the average shear modulus, σ the shear stress on the slip plane and *n* has the value of 3. This is the same form as the equation deduced by Steinemann (1954) from experimental deformation ($\dot{\epsilon}_s = A\sigma^n$). From easy glide experiments at -2°C and 0.1 MPa on the slip plane, $\Lambda_{max} = 0.03$, $\tau_m = 1.5\times10^{-5}\ s^{-1}$ and $G = 3\times10^3$ MPa. When these values are substituted into equation 6 the steady state creep rate equals $1.3\times10^{-5}\ s^{-1}$.

Weertman (1963) also suggests that creep may occur via dislocation climb. This process is much slower than basal glide. It involves the transport of water molecules from the extra half plane of the dislocation to a plane perpendicular to the glide plane. Climb occurs progressively by the migration of jogs on the dislocation. The activation energy for glide controlled by climb in ice is 0.57 eV (Hobbs 1974).

By Chris Wilson and Brett Marmo

2.10 Critical resolved shear stress

Crystalline slip results from the action of a shear stress on the slip plane. Within the range of stresses in natural situations, the component of stress normal to the slip plane does not influence slip. Thus the slip process must be considered in terms of the shear stress resolved on the slip plane in the slip direction. Consider a single crystal of cross-sectional area *A* under a tensile force *F* (Fig. 2.10.1). Let ϕ be the angle between the slip plane normal and the compression axis, and λ the angle between the slip direction and the tensile axis. The component of the applied force, acting in the slip direction is $F\cos\lambda$, and the area of the slip plane is $A/\cos\phi$. The shear stress resolved in the slip direction is then

$$\tau = \frac{F\cos\lambda}{A/\cos\phi} = \sigma\cos\phi\cos\lambda$$

where σ is the applied tensile stress *F/A*.

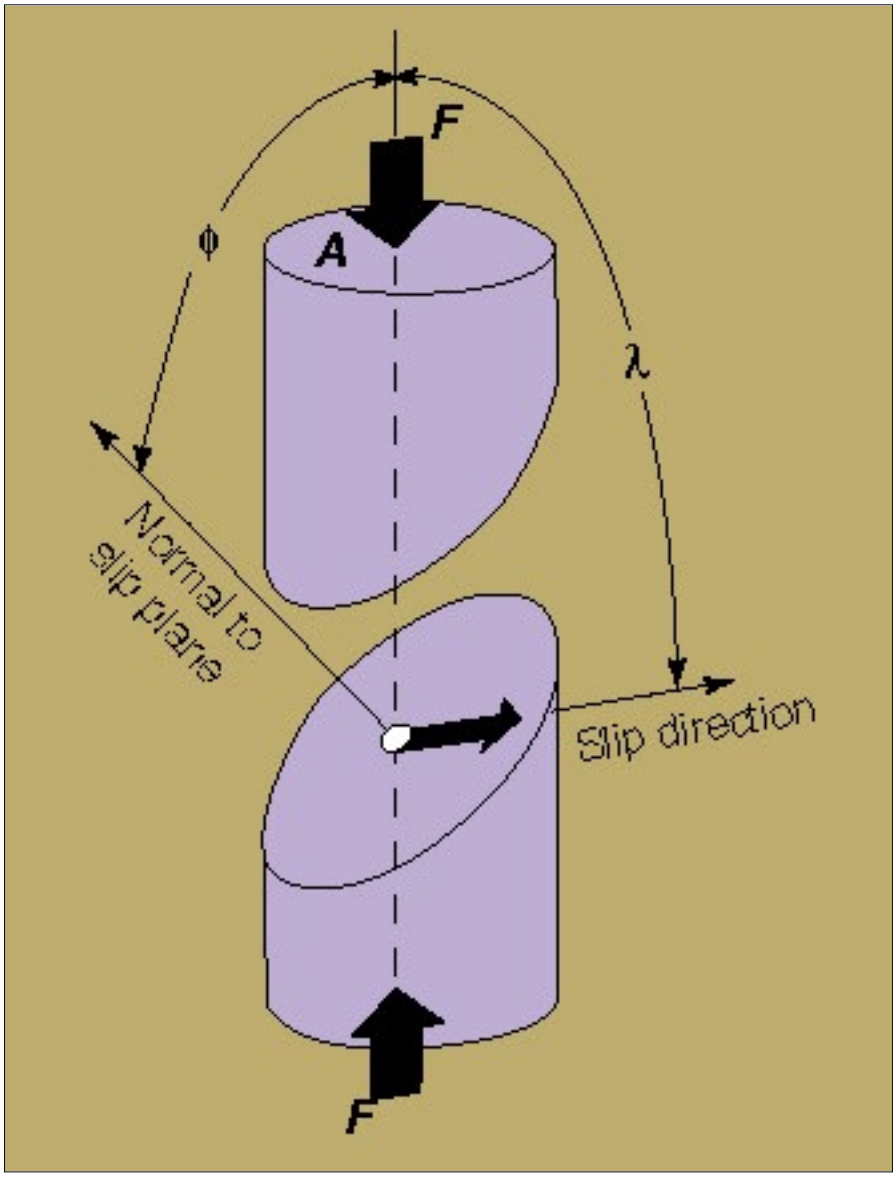

Figure 2.10.1:Two separated portions of a crystal showing a model for calculating the resolved shear stress in a single-crystal specimen. *F* is the applied force, *A* is the cross-sectional area of the specimen, ϕ is the angle between the normal-to-the-slip plane and the compression axis, and λ is the angle between the slip direction and the compression axis.

The stress required to initiate slip in a pure and perfect single crystal, the critical resolved shear stress (CRSS) is a constant for a material at a given temperature. This rule, known as Schmid's Law, has been experimentally proven for a large number of single crystals. The critical stress required to cause yielding is a function of $\cos\phi \cos\lambda$ or the Schmid factor. The slip plane with the greatest resolved shear stress acting upon it will predominate in the slip process.

FLOW IN POLYCRYSTALLINE ICE

Part 2 - Background information

By Chris Wilson and Brett Marmo

2.12 Diffusional flow

If temperature is sufficiently high, even a small stress will induce a flux of matter through or around the boundary of an ice grain. Diffusional flow has been extensively modeled and there is general agreement on the form of the relation describing the strain rate:

$$\dot{\gamma} = \frac{A_{tv}\,\sigma\Omega}{kTd^2} D_{eff}$$

---------- equation (8)

where:

$$D_{eff} = D_v\left(1 + \frac{\pi\delta}{d}\frac{D_b}{D_v}\right)$$

---------- equation (9)

where D_b and D_v are the lattice and grain boundary diffusion coefficients respectively, A_{tv} is a dimensionless constant, Ω is the molecular volume, k is Boltzmann's constant, d is the grain size and δ is the grain boundary width. Diffusional flow in ice has not been well studied as diffusion through the ice lattice is very slow and the grain size large compared to metals and ceramics. Transient creep processes, such as grain boundary sliding and dislocation motion, mask diffusional processes at low strains. Glide related deformation occurs significantly faster that diffusion, but dislocations require a stress greater than 340 Pa to propagate through the ice structure (Goodman et al. 1981). Thus, diffusional flow dominates deformation at low stress but is obscured by the glide at moderate stresses.

By Chris Wilson and Brett Marmo

2.11 Non-basal glide

When a load is applied to an ice crystal such that there is no resolved shear stress on the basal plane, the rate of deformation is so slow that it is extremely difficult to detect. The propagation of dislocations through non-basal systems is not well understood, however deformation experiment on monocrystals by Nakaya (1958), Wakahama (1966), and Higashi (1966) indicate that non-basal systems require at least two orders of magnitude more stress to initiate glide that basal systems (Fig. 2.11.1). Hutchison (1977) suggests that glide may occur on both prismatic $\{01\bar{1}0\}$ $<2\bar{1}\bar{1}0>$ and pyramidal $\{11\bar{2}2\}$ $<11\bar{2}3>$ slip systems (Fig. 1.1.2). Weertman (1973) estimates that non-basal glide is 100 - 1000 time more difficult that basal systems, while Castelnau et al. (1996) suggests that the prismatic slip system requires 20 times more resolved shear stress to initiate glide than the basal systems and the pyramidal systems require 200 time more resolved shear stress than basal systems (Fig. 1.1.2).

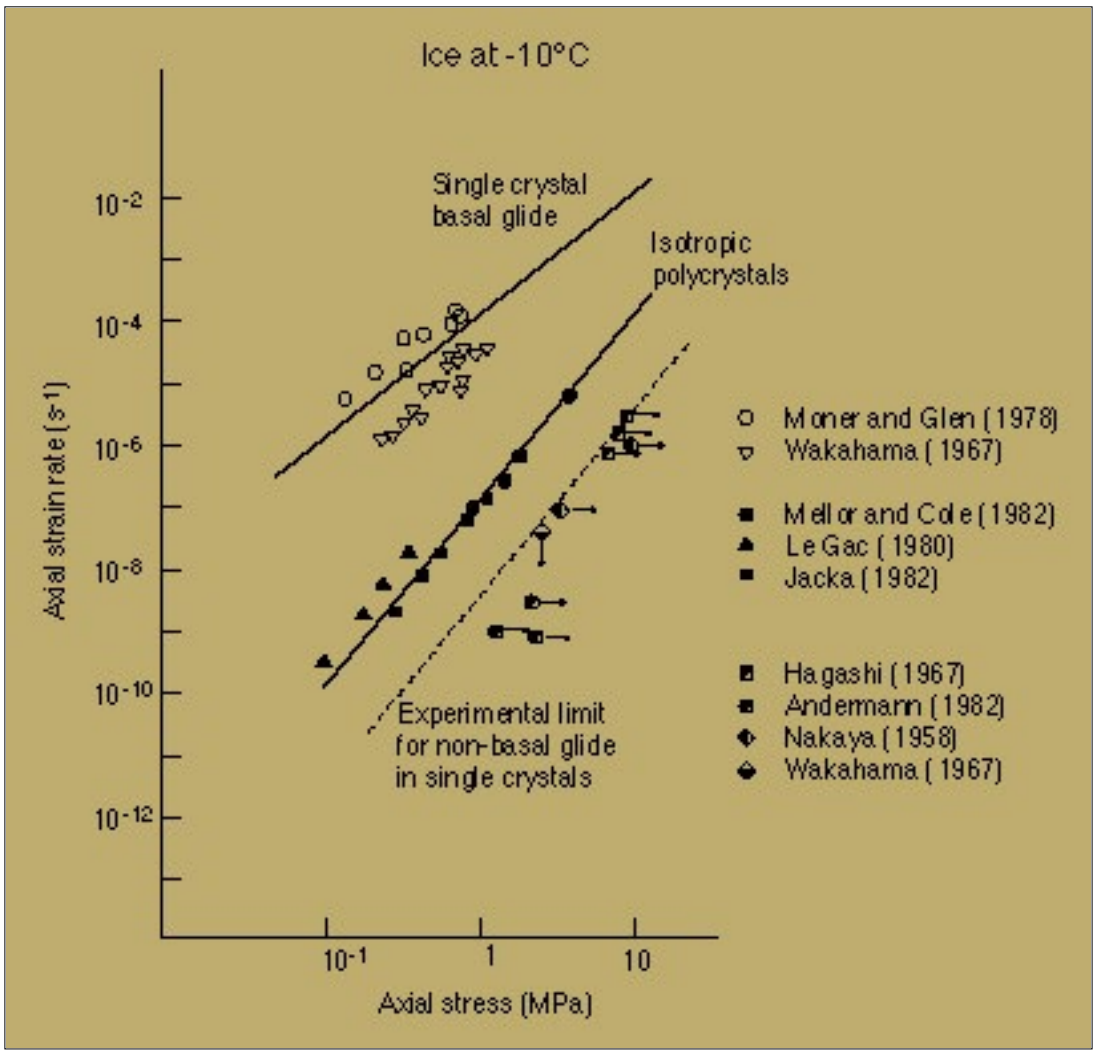

Figure 2.11.1: Data for glide on basal and non-basal systems, and in isotropic polycrystalline ice compiled by Duval et al. (1983). Non-basal glide data shows the low boundary for stress giving rise to deformation and may not represent the true stress required for the observed strain rates.

2.13 Plastic deformation

Glide and diffusional processes also play significant roles in the plastic deformation of polycrystalline ice. Compression experiments show that polycrystalline ice deforms instantly when a stress is applied suddenly (Barnes et al. 1971; Kamb 1972). Initially the strain rate slows with increasing strain; this is known as *primary creep* (Fig. 2.9.2). This reduction in strain rate reflects work hardening similar to that observed in a single crystal of ice that is being deformed in a hard glide orientation (see 2.9 Strain rate for glide on basal systems). Eventually the strain rate becomes constant; this is *secondary creep*, the minimum strain rate. Secondary creep is of principal interest as it gives rise to the steady state flow observed in glaciers. When the compressive stress exceeded a critical stress the strain rate increased significantly. This is known as *tertiary creep* and is due to recrystallisation of ice. Other complicating factors in the deformation of polycrystalline ice are grain boundary melting, pressure melting (Wilson et al. 1996) and the development of crystallographic fabrics which may enhance the flow of the ice.

In order that a polycrystalline solid can deform homogeneously into any arbitrary shape, with no volume change and maintain strain compatibility it must have at least five independent slip systems (Taylor 1938). If uniform strain is not pre-supposed then the polycrystals only require four independent systems (Hutchison 1976). The basal plane of ice crystals provides only two systems. The other two independent systems must be non-basal, but glide is 2 or 3 orders of magnitude more difficult to activate than for basal systems. The non-basal system therefore plays a major role in macroscopic behaviour making deformation of polycrystalline ice slower than that of a single ice crystal (Fig. 2.11.1). The additional non-basal system are most probably the prismatic systems $\{01\bar{1}0\}$ $<2\bar{1}10>$ and pyramidal $\{11\bar{2}2\}$ $<11\bar{2}3>$ slip systems (Fig. 1.1.2). The other possibility is that movement of dislocations on the two independent systems in the basal plane gives rise to dislocation climb normal to the basal plane; and provides a further two systems (Ashby & Duval 1985).

2.18 Grain growth

The average grain-size of a population of deformed crystals in any highly deformed aggregates tends to increase with time. Grain growth is driven by neighbouring grains that possess different energy levels due to the curvature of energetic grain boundaries and/or different amounts of accumulated strain energy. A change in the average grain-size of a polycrystalline aggregate has significant implications for the way the body deforms, as diffusional flow and grain boundary sliding are grain-size dependent. Under certain stress and temperature conditions a progressive increase in grain-size can move the ice from diffusion flow controlled creep to glide controlled creep and from ductile deformation to brittle deformation (Cole 1985).

Surface tension across a curved boundary between two grains gives rise to a pressure difference, with the grain that possesses the concave boundary having a higher energy state. Molecules tend to move from the high energy side of the boundary to the low energy side. This leads to grain boundary migration as the low energy crystal consumes the high energy crystal (Alley 1992). The process decelerates with time because the size of the high energy crystal is reduced which increases the curvature of the boundary and the differential energy between to the two grains. Grain growth driven by curvature of boundaries would continue indefinitely if it were not for the presence of impurities, dust and bubbles which pin grain boundary migration (Alley et al. 1986).

Dislocations and other defects that stem from deformation of a crystal lattice, increase a grain's disorder and internal energy. When a boundary separates a strained crystal from an unstrained crystal, the free energy of the strained crystal is higher. The grain boundary begins to migrate to reduce the total energy of the system, with molecules moving from the strained grain to the unstrained grain. Once this process has begun it will tend to continue as the ice on the unstrained side is newer, more ordered and has a lower energy that the strained crystal (Alley et al. 1986). Eventually the strained grain is reduced in size to the extent that curved boundary effects become significant and the

strained grain is rapidly consumed. In this manner the deformed grains are removed from the ice and the average grain-size is increased with time.

2.19 Grain size reduction

While grains are consumed by boundary migration, they can also be created by recrystallisation and *polygonisation*. Polygonisation is the subdivision of large grains into smaller grains and is driven by different parts of a crystal being subjected to different stress states. The variation in the stress field can lead to a lattice becoming warped or to the development of kink bands orthogonal to the basal plane. Dislocations tend to accumulate at kinks in the lattice which then become the sites for dynamic recrystallisation and the division of crystals into sub-grains (Wilson 1986). Initially subgrains have a small mis-match in crystallographic orientation, but continued deformation leads to rotation of grains and the refinement of boundaries between subgrains. This process is referred to as *rotation recrystallisation* (Poirier 1985) and leads to the subgrains becoming distinctly different crystals.

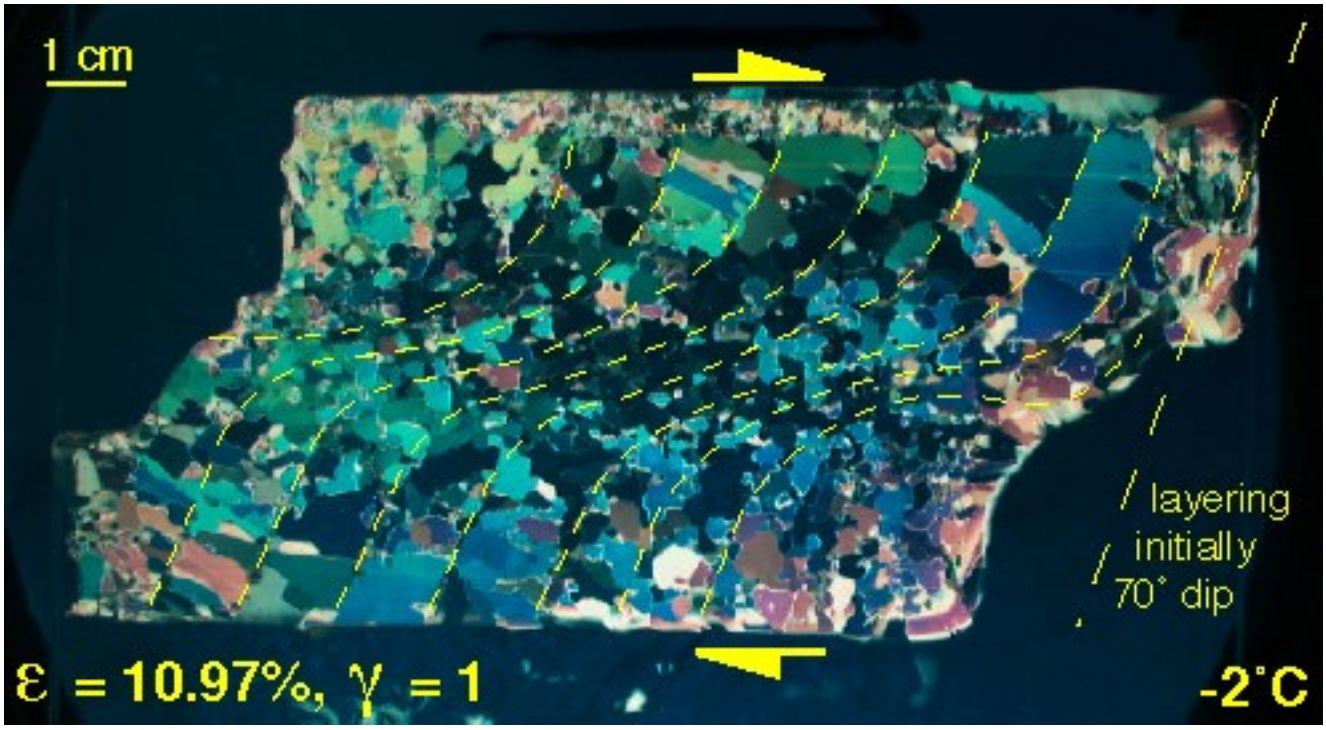

Figure 2.19.1: Grain size reduction occurs in a shear zone developed in coarse ice deformed at -2°C. A compression (applied to the upper surface) and simple shear are applied simultaneously with the shear strain confined to a ~15mm wide zone, bounded by undeformed region. Within the shear zone there is rotation of the pre-existing foliation and substantial grain size reduction.

By Chris Wilson and Brett Marmo

2.17 Deformation mechanism maps

Deformation maps describing mechanisms through which ice deforms have been calculated by Goodman et al. (1981), Frost & Ashby (1982), Duval et al. (1983) and Ashby & Duval (1985). The maps show the region, within stress-temperature space, where one of the flow mechanisms is dominant. Maps are generally plotted with the microscale variables, including grain size, held as constants. The upper boundary of the maps is defined by the region of brittle failure for ice. Figure 16 shows deformation maps for the grain sizes 0.1mm, 1mm and 10mm. Diffusional flow and glide controlled flow form two broad classes of mechanisms through which ice deforms.

Lines of strain rate are also mapped onto the diagrams. The strain rate for each component is calculated from the respective steady state flow laws. As diffusional flow and glide mechanisms occur concurrently the maps show the total strain rate:

$$\dot{\gamma}_{TOTAL} = \dot{\gamma}_{diffusion} + \dot{\gamma}_{glide}$$

The maps have three major regions: a low stress region dominated by diffusional flow; a moderate stress region where glide controlled creep dominates; and a high temperature - high stress area dominated by pressure melting. At high temperatures both recrystallisation and grain boundary melting contribute to the deformation.

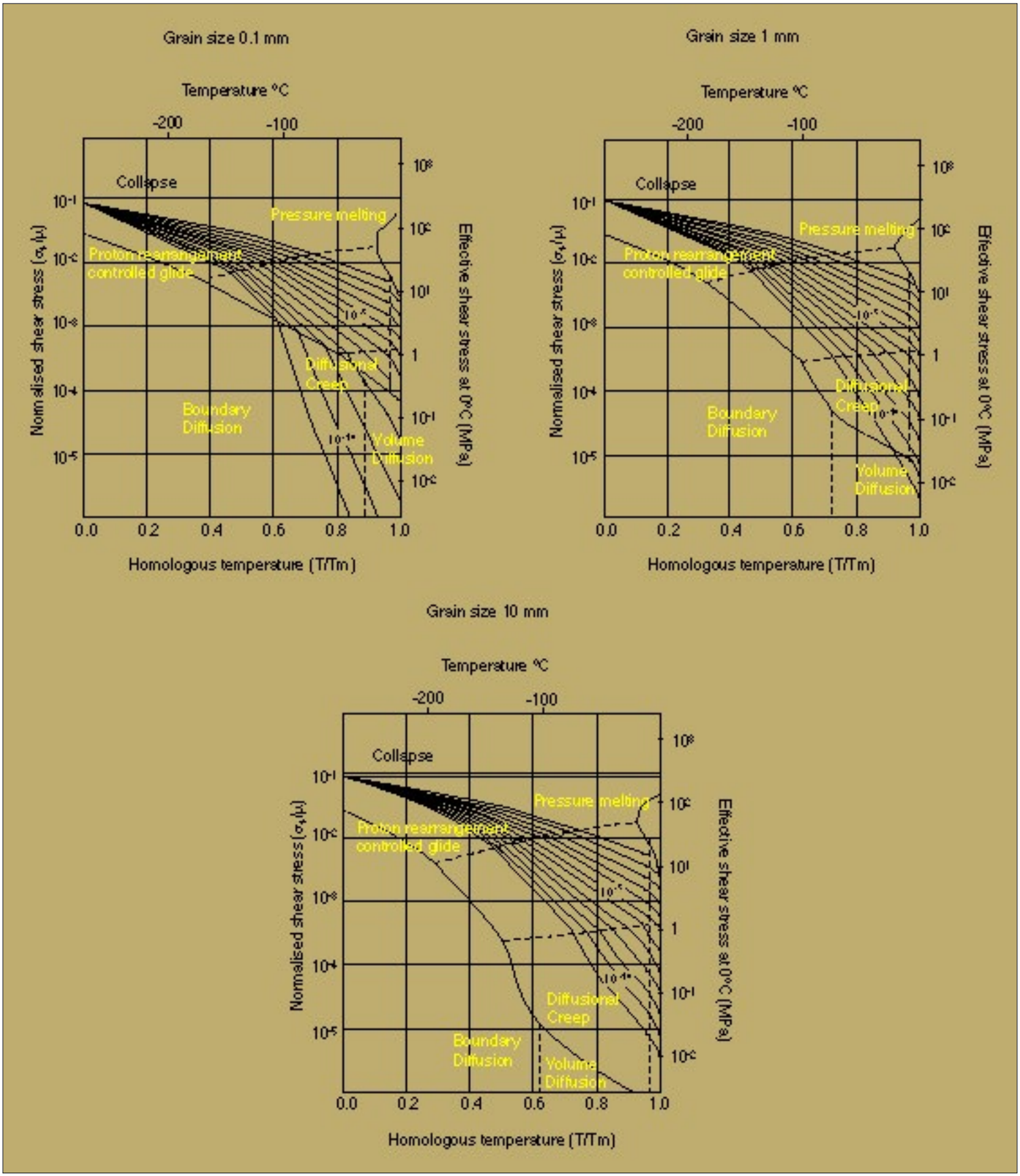

Figure 2.17.1: Deformation mechanism maps for isotropic polycrystalline ice by Goodman et al. (1981). The fields show the deformation process that dominates, given the temperature and stress conditions, and do not indicate that these are the only processes active. The strain rate contours represent the cumulative strain for all processes contributing to deformation. Each contour represents one order of

magnitude in s^{-1}. Note the variation in each field for different mean grain sizes.

FLOW IN POLYCRYSTALLINE ICE

Part 1 - Examples of microscopic flow

By Chris Wilson and Brett Marmo

1.7 References

Ahmad, S., Ohtomo, M. & Whitworth, R. W. (1986). Observations of a dislocation source in ice by synchrotron radiation topography, *Nature* **319**: 659-660.

Ahmad, S., Shearwood, C. & Whitworth, R. W. (1992). Dislocation multiplication mechanisms in ice, In *Physics and Chemistry of Ice* (ed. N. Maeno and T. Hondoh), pp. 492-6. Hokkaido University Press, Sapporo.

Alley, R. B. (1992). Flow-law hypotheses for ice-sheet modeling, *Journal of Glaciology*. **38**: 245-256.

Alley, R. B., Perepezko, J. H. & Bentley, C. R. (1986). Grain growth in polar ice: I. Theory, *Journal of Glaciology* **32**: 415-424.

Ashby, M. F. & Duval, P. (1985). The creep of polycrystalline ice, *Cold Regions Science and Technology* **11**: 285-300.

Azuma, N. & Higashi, A. (1985). Formation processes of ice fabric patterns in ice sheets, *Annals of Glaciology* **6**: 130-134.

Azuma, N. (1994). A flow law for anisotropic ice and its implication to ice sheets, *Earth and Planetary Science Letters* **128**: 601-614.

Azuma, N. (1995). A flow law for anisotropic ice under uniaxial compressive deformation, *Cold Regions Science and Technology* **23**: 137-147.

Azuma, N. & Goto-Azuma, K. (1996). An anisotropic flow law for ice-sheet ice and its implications, *Annals of Glaciology* **23**:202-208.

Baker, I. (1997). Observation of dislocations in ice. *Journal of Physical Chemistry* **B 101**: 6158-6162.

Barnes, P., Tabor, D. & Walker, J. C. F. (1971). The friction and creep of polycrystalline ice, *Proceedings of the Royal Society of London* **A125**: 670-693.

Bernal, J. D. & Fowler, R. H. (1933). A theory of water and ionic solution, with particular reference to hydrogen and hydroxyl ions, *Journal of Chemistry and Physics* **38**: 840-846.

Bjerrum, N. (1951). Structure and properties of ice i. the position of hydrogen atoms and the zero-point entropy of ice, *K. danske Vidensk. Selsk. Skr*. **27**: 56.

Bridgman, P. W. (1937). The phase diagram of water to $45000\ kg/cm^2$, *Journal of Chemistry and Physics* **5**: 964-966.

Budd, W. F. & Jacka, T. H. (1989). A review of ice rheology for ice sheet modeling. *Cold Regions Science and Technology*, **16**, 107-44.

Castelnau, O., Thorsteinsson, T., Kipfstuhl, J., Duval, P. & Canova, G. R. (1996). Modeling fabric development along the GRIP ice core, central Greenland, *Annals of Glaciology* **23**: 194-201.

Coble, R. L. (1963). A model for boundary diffusion controlled creep in polycrystalline materials, *Journal of Applied Physics* **34**: 1979-1982.

Cole, D. M. (1985). Grain growth and the creep behaviour of ice, *Cold Regions Science and Technology* **10**: 187-189.

Duval, P., Ashby, M. F. & Anderman, I. (1983). Rate controlling processes in the creep of polycrystalline ice, *Journal of Physical Chemistry* **87**: 4066-4074.

Eshelby, J. D. (1961). Dislocations in visco-elastic materials, *Philosophical Magazine* **6**: 953-963.

Frost, H. J. & Ashby, M. F. (1982). *Deformation-mechanism maps. The plasticity and creep of metals and ceramics*, Published by Pergamon Press, New York.

Glen, J. W. (1955). The creep of polycrystalline ice, *Proceeding of the Royal Society* **A228**: 513-38.

Glen, J. W. (1968). The effects of hydrogen disorder on dislocation movement and plastic deformation of ice, *Physics of condensed matter* **7**: 43-51.

Glen, J. W. & Perutz, M. F. (1954). The growth and deformation of ice crystals, *Journal of Glaciology* **2**: 397-403.

Goldsby, D. L. & Kohlstedt, D. L. (1997). Grain boundary sliding in fine-grained ice I. *Scripta Materialia*, **37**, 1399-406.

Goodman, D. J., Frost, H. J. & Ashby, M. F. (1981). The plasticity of polycrystalline ice, *Philosophical Magazine* **43**: 665-695.

Griggs, D. T. & Coles, N. E. (1954). Creep of a single crystal of ice, *SIPRE Technical Report* **11**: 24.

Herring (1950). Diffusional viscosity of a polycrystalline solid, *Journal of Applied Geophysics* **21**: 437.

Higashi, A. (1966). Mechanisms of plastic deformation in ice single crystals, *Physics of ice and snow Conference Proceeds* **1**: 277.

Hobbs, P. V. (1974). *Ice Physics*, Clarendon Press, Oxford.

Hudleston, P. J. (1980). The progressive development of inhomogeneous shear and crystallographic fabric in glacial ice, *Journal of Structural Geology* **2**: 189-196.

Hutchison, J. W. (1976). Bonds and self consistent estimates for creep of polycrystal materials, *Proceedings of the Royal Society of London* **A348**: 101-127.

Hutchison, J. W. (1977). Creep and plasticity of hexagonal polycrystals as related to single crystal slip, *Met Trans* **8A**: 1465-1469.

Jacka, T. H. (1984). The time and strain required for development of minimum strain rates in ice. *Cold Regions Science and Technology*, **8**, 261-8.

Jia, K., Baker, I., Liv, F. & Duddley, M. (1996). Observation of slip transmission through a grain boundary in ice. *Journal of Material Science*, **31**: 2373-2378.

Jones, S. J. & Glen, J. W. (1969). The effect of dissolved impurities on the mechanical properties of ice crystals, *Philosophical Magazine* **19**: 13-24.

Kamb, W. B. (1959). Ice petrofabric observations from Blue Glacier, Washington in relation to theory and experiment, *J. Geophys. Res.*, **64**, 1891-1909.

Kamb, W. B. (1961). The glide direction in ice, *Journal of Glaciology.*, **3**, 1097-1106.

Kamb, W. B. (1972). Experimental recrystallization of ice under stress, *Am. Geophys. Union Monog.*, **16**, 211-241.

Liv, F., Baker, I. & Duddley, M. (1995). Dislocation-grain boundary interactions in ice crystals. *Philosophical Magazine* **A71**: 15-42.

McConnell, J. C. (1891). On the plasticity of an ice crystal, *Proceedings of the Royal Society of London* **49**: 323-343.

Manley, M. E. & Schulson E. M. (1997). On the strain-rate sensitivity of columnar ice. *Journal of Glacialogy*, **43**, 408-10.

Marmo, B. & Wilson, C. J. L. (1998). Strain localisation and incremental deformation within ice masses, Framnes Mountains, east Antarctica. *Journal of Structural Geology*, **20**: 149-162.

Marmo. B. & Wilson, C. J. L. (1999). A verification procedure for the use of FLAC to study glacial dynamics and the implementation of an anisotropic flow law. *FLAC and Numerical Modeling in Geomechanics* (eds. Detournay, C. & Hart, R.), pp183-190. Balkema, Rotterdam.

Mellor, M. & Cole, D. M. (1982). Deformation and failure of ice under constant stress or constant strain-rate. *Cold Regions Science and Technology*, **5**: 201-19.

Nabarro, F. R. N. (1948). Deformation of crystals by motion of a single ions. In *Strength of solids. Report of a conference on the Strength of Solids, Bristol 7th-9th July 1947* (ed. N. F. Mott) Physical society, London. p. 75-90.

Nakaya, U. (1958). *Mechanical properties of single crystals of ice. Part I. Geometry of deformation*, US Army Snow, Ice and Permafrost Research Establishment Research Report no. 28.

Nye, J. F. (1952). The mechanics of glacier flow. *Journal of Glaciology*, **2**, 82-93.

Petrenko, V. F. & Whitworth, R. W. (1999). *Physics of Ice*, Oxford University Press.

Pimienta, P., Duval, P., & Lipenkov, V. Y. (1987). Mechanical behaviour of anisotropic polar ice, *IAHS Publications* **170**: 57-66.

Poirier, J -P. (1985). *Creep of Crystals*, Cambridge University Press.

Rigsby, G. P. (1957). Effects of hydrostatic pressure on velocity of shear deformation of single crystals of ice, *SIPRE Technical Report* **32**: 7.

Pauling, L. (1935). The structure and entropy of ice and of other crystals with some randomness of atomic arrangement, *Journal of American Chemistry and Physics* **57**: 2680-2684.

Rist, M. A. & Murrell, S. A. F. (1994). Ice triaxial deformation and fracture. *Journal of Glaciology*, **40**, 304-18.

Schoeck, G. (1956). Moving dislocations and solute atoms, *Physics Review* **102**: 1458-1459.

Shearwood, C. & Whitworth, R. W. (1991). The velocity of dislocations in ice, *Philosophical Magazine* **64**: 289-302.

Steinemann, S. (1954). Results of preliminary experiments on the plasticity of ice, *Journal of Glaciology* **2**: 404-412.

Taylor, G. I. (1938). Plastic strain in metals, *Journal of the Institute of Metals* **62**: 307-24.

Van der Veen, C. J. & Whillans, I. M. (1994). Development of fabric in ice, *Cold Regions Science and Technology* **22**: 171-195.

Wakahama, G. (1962). On the plastic deformation of ice, *Low Temperature Science* **A20**: 57-130.

Wakahama, G. (1966). On the plastic deformation of single crystal of ice, *Physics of ice and snow Conference Proceedings* **1**: 291.

Weertman, J. (1963). The Eshelby-Shoeck viscous dislocation damping mechanism applied to steady state creep of ice. In *Ice and Snow: properties, processes and applications* (ed. W. D. Kingery), pp. 28-33. MIT Press,

Cambridge, Massachusetts.

Weertman, J. (1973). Creep of ice. In *Physics and chemistry of ice* (ed. E. Whalley, S. J. Jones, and L. W. Gold), pp. 320-337. Royal Society of Canada, Ottawa.

Weertman, J. & Weertman, J. R. (1964). *Elementary dislocation theory*, Macmillan, New York.

Whitworth, R. W. (1978). The core structure and mobility of dislocations in ice, *Journal of Glaciology* **21**: 341-59.

Wilson, C. J. L. (1986). Deformation induced recrystallisation of ice: The application of in situ experiments. In *Mineral and rock deformation laboratory studies* (ed. Hobbs, B. E. & Heard, H. C.), American Geophysical Union (Geophysical Monograph **36**), pp. 213-234

Wilson, C. J. L. & Russell-Head, D. S. (1982). Steady-state preferred orientation of ice deformed in plane strain at -1°C, *Journal of Glaciology* **28**: 145-159.

Wilson, C. J. L., Zhang, Y. & Stuwe, K. (1996). The effects of localized deformation on melting processes in ice, *Cold Regions Science and Technology* **24**: 177-189.

Wilson, C.J.L. & Zhang, Y. (1996). Development of microstructure in the high-temperature deformation of ice, *Annals Glaciology*, **23**: 293-302.

Wilson, C.J.L. & Zhang, Y. (1994). Comparison between experiment and computer modeling. of plane-strain simple-shear ice deformation, *J Glaciology*, **40**: 46-53.

FLOW IN POLYCRYSTALLINE ICE

Part 1 - Examples of microscopic flow

By Chris Wilson and Brett Marmo

1.8 Acknowledgments

We thank Win Means for the inspiration over the years for continually asking the right questions and for the opportunity he gave Chris to work in his laboratory. We thank Hadi Sim for all his help in getting this presentation together. The research was supported by the Australian Research Council Grant A39601139 and support from the Australian Antarctic Division.

2.4 Bernard-Fowler rule

The Bernal-Fowler rule allows the rotation of water molecules within the Ice *Ih* lattice by hydrogen atoms jumping sites. This movement requires that all hydrogen atoms move simultaneously or the presence of point defects. Bernal & Fowler (1993) suggested that a single hydrogen atom lies on a line between each oxygen atom. The angle between oxygen atoms within Ice *Ih* is 109°, thus only a small variation of the H-O-H angle in the gas phase is necessary to accommodate hydrogen in the Ice *Ih* lattice. The hydrogen atoms lie 1Å from their associated oxygen atoms and 1.76Å from the closest neighbouring oxygen atom. There are six possible configurations of hydrogen atoms around oxygen atoms that satisfy this arrangement.

A statistical model of the position of hydrogen atoms was produced by Pauling (1935) based on the six possible configurations of hydrogen atoms within Ice *Ih*. The statistical model is known as the Bernard-Fowler rule and is defined as ideal crystal based on the assumptions that:

1. Each oxygen atom is bonded to two hydrogen atoms at a distance of 0.95Å to form a water molecule;
2. Each molecule is orientated so that its two hydrogen atoms face two, of the four, neighbouring oxygen atoms that surround in tetrahedral coordination;
3. The orientation of adjacent molecules is such that only one hydrogen atom lies between each pair of oxygen atoms;
4. Ice *Ih* can exist in any of a large number of configurations, each corresponding to a certain distribution of hydrogen atoms with respect to oxygen atoms.

There is an electrostatic attraction between the positively charged hydrogen nucleus ($+e_0$) of one molecule and the negatively charged lone pair ($-2e_0$) of a

neighbouring molecule. Hydrogen atoms therefore are most stable when aligned along an axis parallel to a neighbour's lone pair. The electrostatic attraction increases the distance from the oxygen atom and its associated hydrogen atoms from 0.96Å (in the gas phase) to 1.011Å. The lattice energy, *L*, for Ice *Ih* is the difference between the energy of a motionless water molecule in the gas phase at 0°K and its energy in Ice *Ih* at 0°K. The lattice energy for Ice *Ih* is L=0.58 eV (Hobbs 1974). If the lattice energy is attributed to hydrogen bonding, then the energy of the hydrogen bond will be half the value of the lattice energy (as each molecule contains two hydrogen atoms). Thus the energy of the hydrogen bond is 0.29 eV.

FLOW IN POLYCRYSTALLINE ICE

Part 2 - Background information

By Chris Wilson and Brett Marmo

2.14 Primary Creep

When a load is initially applied to a polycrystalline aggregate, both grains in easy glide and hard glide orientations deform elastically (Fig. 2.14.1, AB). With increasing stress the easy glide grains begin to glide and plastically deform. As the easy glide grains relax, stress is redistributed onto the hard glide grains which are progressively rotated and begin to deform in an elastic-plastic manner. If the stress is removed at this point, some but not all of the strain is recoverable, as the easy glide grains have deformed permanently. If the stress is continued then, hard glide grains will eventually begin to fail by plastic deformation and contribute to the bulk deformation at which point secondary glide is achieved.

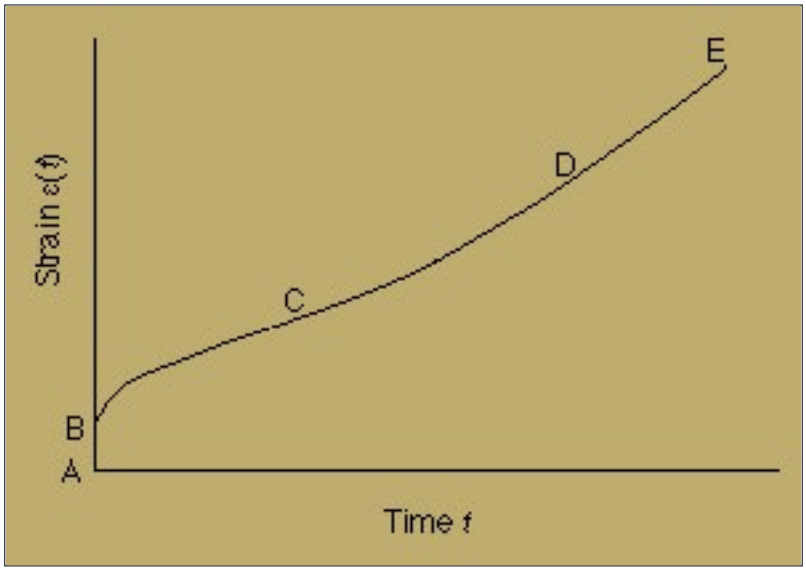

Figure 2.14.1: Schematic creep curve for polycrystalline ice under constant load.

The region of decelerating "primary creep" extends from B to the inflection point C, after which the creep accelerates and eventually reaches a constant rate DE. Early work on ice by Glen (1955) and Barnes et al. (1971) identified a region of steady-state or "secondary creep" around the point C. Later experiments show only a broad minimum in $\dot{\varepsilon}(t)$, but the minimum strain rate

$\dot{\varepsilon}_{min}$ represents a very important quantity in the analysis of the creep data. Deformation beyond the minimum is called "tertiary creep". The final steady state $\dot{\varepsilon}_{max}$ marked DE in Fig. 2.14.1 is hard to attain in laboratory experiments, but this is the region of most significance in geology and glaciology.

2.15 Secondary Creep

True steady-state secondary creep is not observed in ice. Figure 2.15.1 shows examples at -17.8°C from the many creep curves obtained by Jacka (1984), plotted here in the form of strain rate as a function of strain using logarithmic scales. These curves show well-developed minima, but note that to achieve the minimum at the lowest stress the deformation had to be followed for more than a year! Many early experiments did not reach the strain rate minimum, and secondary creep rates reported in the literature may be misleading. Nevertheless secondary creep rates, whether obtained at the true minimum or not, have been extensively used in making comparisons between experiments performed at different stresses and temperatures. The important thing about the point of inflection C on the creep curve (Fig. 2.14.1) is not the balance between decelerating primary creep and accelerating tertiary creep. It is that in this approximately steady-state situation plastic flow of the grains occurs at a rate that is in balance with the processes which relieve the internal stresses so produced. These processes, which may include dislocation climb and grain boundary sliding or migration, are the rate limiting factors for secondary creep in polycrystalline ice.

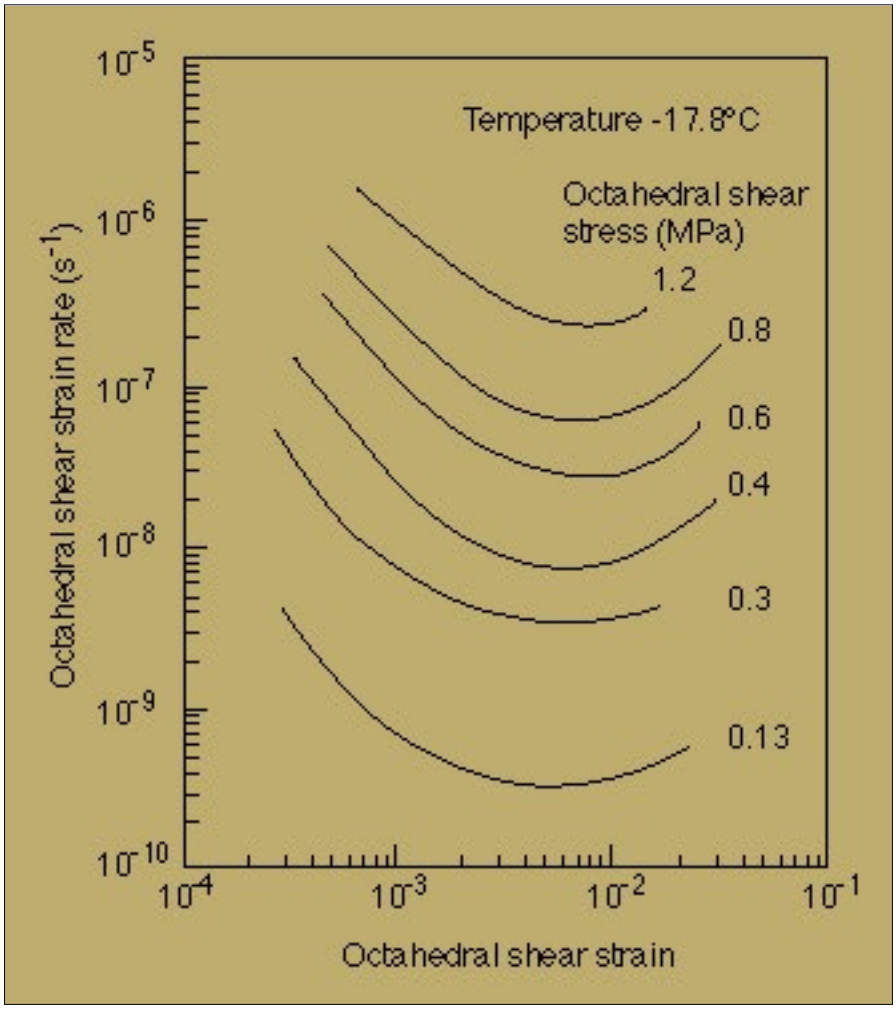

Figure 2.15.1: Plots of strain rate as a function of strain for creep of granular polycrystalline ice in uniaxial compression under various stresses. In this and the following three figures stresses and strains have been converted to octahedral values according to equations in Jacka (1984).

The points plotted in Fig. 2.11.1 are the secondary creep rates of polycrystalline ice deduced in various ways from various tensile and compressive tests at -10°C, and the figure shows that this creep rate is intermediate between those for basal and non-basal slip in single crystals. Over an intermediate range of the stresses shown on the figure the secondary creep of polycrystalline ice obeys the power law proposed by Glen (1955)

$$\dot{\varepsilon} = A\sigma^n$$

where A is a constant and $n \approx 3$. The logarithmic plot of Fig. 2.14.2 includes a line with this slope. In the experiments of Barnes et al. (1971) there was evidence that $n>3$ at high stresses, and more recently Rist & Mureell (1994) obtained $n \approx 4$ from constant strain rate compression tests at high stress. Values of n greater than 3 have often been associated with the formation of microcracks in the ice. However, Manley and Schulson (1997) have produced experimental data suggesting that n is correlated with two-dimensional (glide)

to three-dimensional (glide plus climb) of dislocations.

For the creep curves in Fig. 2.15.1 all the minima occur at the same strain $\varepsilon_{crit} = 0.67 \pm 0.10\%$ (equivalent to $\varepsilon = 0.95\%$ in compression). This strain for minimum strain rate is the same within experimental error for temperatures from -5 to -32.5°C in the experiments of Jacka (1984) and Mellor & Cole (1982). The dependence of the minimum strain rate $\dot{\varepsilon}_{min}$ on stress for various temperatures is shown in Fig. 2.15.2 (Budd and Jacka 1989). These stress dependencies all fit Glen's equation (equation 1) with n=3, and reports of smaller values of n at low stresses are probably consequences of failure to attain the true minimum rate.

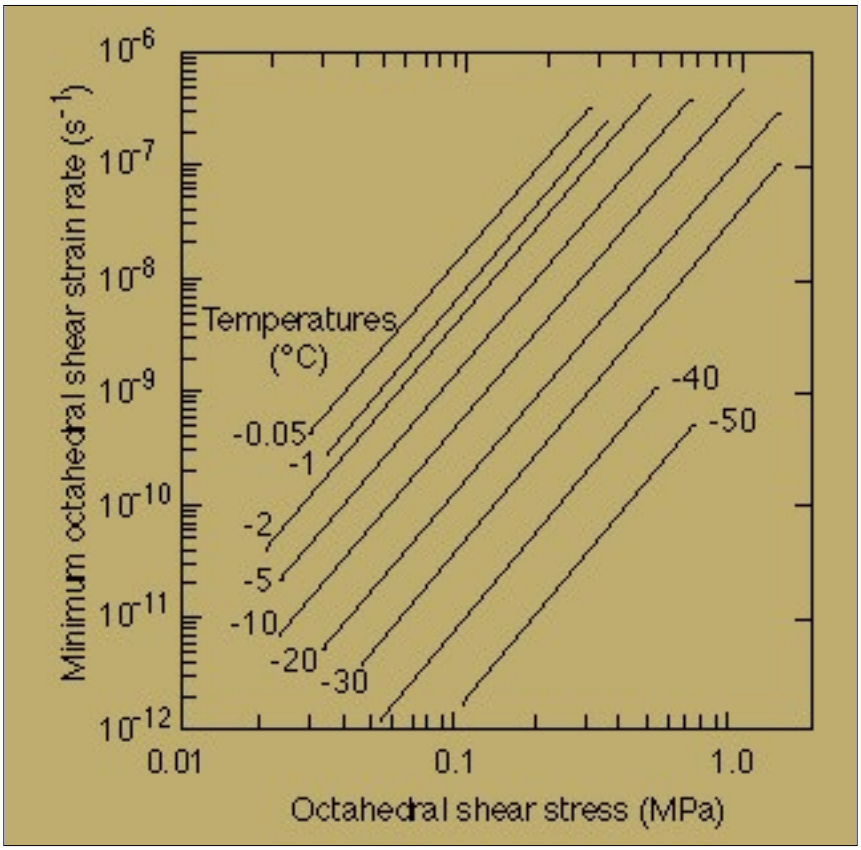

Figure 2.15.2: The minimum strain rate is uniaxial creep tests on granular polycrystalline ice as functions of stress at various temperatures (after Budd and Jacka, 1989).

By Chris Wilson and Brett Marmo

2.16 Tertiary Creep

Duval et al. (1983) have demonstrated that the acceleration of creep in polycrystalline ice is at least partially due to the formation of microcracks within polycrystalline ice. The microcracks are about equal to the grain size and their density increase with strain. The initiation and movement across microcracks results in additional stresses on uncracked crystals which produces localised internal stress variations. Duval et al. (1983) also showed that a sample deformed at 1.86 MPa had a steady increase in microcrack initiation that resulted in a concurrent increase in strain rate, while a sample that was deformed under 1 MPa increased in strain rate without any observed cracking which indicates that microcracking is not the only process that produces tertiary creep.

Dynamic recrystallisation also contributes to tertiary creep. Recrystallisation induces the development of a preferential *c*-axis orientation in ice that deforms close to its melting point which results in strain softening and an increase in strain rate. Dynamic recrystallisation occurs as a discontinuous process. At a certain critical strain a wave of recrystallisation will occur and pass through the deforming ice. This is well documented in metals where it occurs at ~20%, whereas within ice it typically occurs at ~1% (Duval et al. 1983).

For a given kind of deformation the ratio of the strain rate for steady-state tertiary creep $\dot{\varepsilon}_{max}$ to the minimum strain rate $\dot{\varepsilon}_{min}$ is found to be a constant independent of both stress and temperature. In uniaxial compression $\dot{\varepsilon}_{max}/\dot{\varepsilon}_{min} \approx 3$, and for simple shear the ratio is ≈ 8 (Budd and Jacka 1989). This shows that the flow processes are similar in both secondary and tertiary creep, with the difference between them arising from the more favourable fabric established in the tertiary stage. In the case of shear the preferred fabric has all grains with their *c*-axes, but in compression the *c*-axes are distributed over a cone, and this is how shear deformation can give a greater enhancement than compression. If ice deformed into the tertiary stage is subsequently tested in a

different orientation it is much more resistant to deformation. Eventually recrystallisation re-orients the fabric to one appropriate to the new stress regime. It is very important to recognize that ice flowing in an ice sheet has highly anisotropic properties that are developed during its recent history.